

Henna Tahvanainen

## **Modelling body vibration and sound radiation of a modified kantele**

**School of Electrical Engineering**

Thesis submitted for examination for the degree of Master of Science in Technology.

Espoo 26.11.2012

**Thesis supervisor:**

Prof. Vesa Välimäki

**Thesis instructor:**

D.Sc. (Tech.) Henri Penttinen



**Aalto University**  
School of Electrical  
Engineering

Author: Henna Tahvanainen

Title: Modelling body vibration and sound radiation of a modified kantele

Date: 26.11.2012

Language: English

Number of pages:8+65

Department of Signal Processing and Acoustics

Professorship: Acoustics and Audio Signal Processing

Code: S-89

Supervisor: Prof. Vesa Välimäki

Instructor: D.Sc. (Tech.) Henri Penttinen

In this thesis, the vibrational modes and radiation of the body of a 15-string instrument called the kantele are modelled using the finite element method. Two traditional body structures, the top-plate kantele and the box kantele, are compared to a modified kantele with an air gap separating the top and the back plate. The modified structure allows the kantele top plate to vibrate freely. In addition, together the top and back plate create an enclosed air mass that has its own vibrational modes. The modified kantele has previously been shown to be louder than the traditional top plate kantele.

In this thesis, it is shown that the modified kantele includes vibrational modes of both the freely vibrating top plate and the enclosed air. Thus, it has a higher mode density than the traditional kanteles. Because of the coupling of the enclosed air modes to the body, the modified kantele radiates more omni-directionally than the traditional kanteles. Consequently, the modified kantele has a higher radiation efficiency than the traditional kanteles when the size of the air gap is small (1-3 mm).

Keywords: Acoustics, Music, Finite Element Methods, Vibrations

Tekijä: Henna Tahvanainen

Työn nimi: Muunnellun kanteleen kopan värähtelyn ja äänisäteilyn  
mallintaminen

Päivämäärä: 26.11.2012

Kieli: Englanti

Sivumäärä:8+65

Signaalinkäsittelyn ja akustiikan laitos

Professori: Akustiikka ja äänenkäsittely

Koodi: S-89

Valvoja: Prof. Vesa Välimäki

Ohjaaja: TkT Henri Penttinen

Tässä työssä mallinnetaan 15-kielisen kanteleen kopan värähtelyä ja säteilyä elementtimenelmän avulla. Kahta perinteistä kopan rakennetta, laatikkokanteletta ja lautakanteletta, verrataan muunnelluun rakenteeseen, jossa kopan ja kannen välillä on ilmarako. Tämä rakenne, jota kutsutaan myös nimellä vapaareuna-erillispohjarakenne, mahdollistaa kannen vapaan värähtelyn. Lisäksi pohjan ja kannen sulkemalla ilmatilalla on omat värähtelymuotonsa. Tämä muunnellun kanteleen on osoitettu olevan äänekkäämpi kuin perinteiset kanteleet.

Tässä työssä osoitetaan, että muunnellussa kanteleessa yhdistyvät sekä kannen että ilmatilan värähtelymuodot. Siksi muunnellulla kanteleella on suurempi värähtelymuototiheys kuin perinteisillä kanteleilla. Muunneltu kantele on myös ympärisäteileivämpi, sillä ilmatilan värähtelymuodot kytkeytyvät kopan värähtelyihin. Tästä seuraa, että muunnellun kanteleen säteilytehokkuus on suurempi, kun ilmarako on pieni (1-3 mm).

Avainsanat: akustiikka, musiikki, elementtimenetelmät, värähtelyt

## Acknowledgements

First of all, I would like to thank my supervisor Prof. Vesa Välimäki, in particular for the valuable comments on the thesis. He made it possible for me to become involved in acoustics in the first place, and to connect my two passions: sound and physics.

As for my instructor, DSc Henri Penttinen, I would like to thank him both for his persistence and patience as well as for the balanced amount of challenge and support in the process.

I would also like to express my gratitude to the mastermind behind the modified kantele, luthier Jyrki Pölkki, and Soitinrakentajat AmF for providing the kantele for the modelling, and for hosting me at the instrument building workshop in Leppävirta. I am thankful for Jyrki for opening my eyes to the instrument builder's point of view.

I would like to add a thank-you to MA Jarno Vesa for helping me to finalise the CAD model of the kantele and to MSc Jussi Hynninen for providing and maintaining the necessary software and hardware for this thesis.

I would like to thank Prof. Jorma Skyttä for being a very understanding superior and allowing me to work on the thesis, and being genuinely interested in the progress. Similarly, I would like to extend my gratitude to the people behind the research team of acoustics and audio signal processing at Aalto University for sharing their passion for acoustics, teaching, music, life, and everything with me. If it wasn't for the inspirational working community, I don't think I would have found my line of work.

To my family and friends, without a doubt, I am grateful. I would like to thank my parents and my brothers for the encouraging words and thoughts.

Finally, I would like to thank Archontis for being there, and showing me what support can mean.

Otaniemi, 21.11.2012

Henna Tahvanainen

# Contents

|   |            |
|---|------------|
| <b>Abstract</b>   | <b>ii</b>  |
| <b>Abstract (in Finnish)</b>  | <b>iii</b> |
| <b>Acknowledgements</b>   | <b>iv</b>  |
| <b>Contents</b>   | <b>v</b>   |
| <b>Symbols and abbreviations</b>  | <b>vii</b> |
| <b>1 Introduction</b>   | <b>1</b>   |
| <b>2 Construction and acoustics of the kantele</b>                            | <b>3</b>   |
| 2.1 Strings . . . . .   | 4          |
| 2.1.1 Ideal string vibration . . . . .  | 4          |
| 2.1.2 Real string vibration . . . . .   | 6          |
| 2.2 Body . . . . .  | 7          |
| 2.2.1 Structure . . . . .   | 7          |
| 2.2.2 Materials . . . . .   | 9          |
| 2.2.3 Plate vibration . . . . .   | 11         |
| 2.3 Coupling between the strings and the body . . . . .                       | 13         |
| 2.4 Coupling between the body and the enclosed air . . . . .                  | 14         |
| 2.5 Coupling between the body and the surrounding air . . . . .               | 15         |
| 2.5.1 Radiated sound power . . . . .  | 15         |
| 2.5.2 Radiation efficiency . . . . .  | 16         |
| 2.5.3 Cancellation of radiation . . . . .                                     | 16         |
| 2.5.4 Power conversion efficiency . . . . .                                   | 17         |
| 2.5.5 Directivity . . . . .   | 18         |
| <b>3 Finite element method in string instrument modelling</b>                 | <b>19</b>  |
| 3.1 The basis of finite element method . . . . .                              | 20         |
| 3.2 Formulation in the structure-acoustic domain . . . . .                    | 21         |
| 3.3 Accuracy and efficiency issues . . . . .                                  | 24         |
| 3.4 Previous work on finite element modelling of string instruments . . . . . | 26         |
| <b>4 Model and measurements of a modified kantele</b>                         | <b>29</b>  |
| 4.1 Model geometry . . . . .  | 29         |
| 4.2 Material properties . . . . .   | 31         |
| 4.3 Boundary conditions . . . . .   | 31         |
| 4.4 Meshing and frequency range . . . . .                                     | 32         |
| 4.5 Force and damping considerations . . . . .                                | 32         |
| 4.6 Measurements . . . . .  | 33         |

|          |   |           |
|----------|---|-----------|
| <b>5</b> | <b>Results</b>  | <b>34</b> |
| 5.1      | Experimental and modelled frequency responses . . . . .   | 34        |
| 5.2      | Structural and material changes . . . . .                 | 36        |
| 5.3      | Comparison of traditional and modified kanteles . . . . . | 39        |
| 5.4      | Effects of different air gap sizes . . . . .              | 43        |
| 5.5      | Radiation efficiency . . . . .                            | 44        |
| 5.6      | Eigenfrequencies and Helmholtz resonance . . . . .        | 47        |
| <b>6</b> | <b>Conclusions and future work</b>                        | <b>48</b> |
|          | <b>References</b>   | <b>50</b> |
| <b>A</b> | <b>Appendix</b>   | <b>56</b> |

# Symbols and abbreviations

## Symbols

|            |   |
|------------|---|
| $A$        | area of the neck of the Helmholtz resonator       |
| $b_s$      | body force on the structure                       |
| $C_s$      | material stiffness matrix                         |
| $c_0$      | speed of sound in air                             |
| $c_i$      | speed of sound in direction $i$ in a material     |
| $d$        | string diameter                                   |
| $d_f$      | displacement of the fluid                         |
| $d_j$      | displacement at the nodal point $j$               |
| $d_s$      | displacement of the structure                     |
| $E_i$      | elastic modulus                                   |
| $F$        | input force                                       |
| $F_b$      | force caused by the body of the structure         |
| $F_d$      | driving point force                               |
| $F_f$      | force caused by surface traction in the structure |
| $F_q$      | force caused by the added mass on the fluid       |
| $F_s$      | force caused by the pressure of the fluid         |
| $f_1, f_2$ | frequencies of coupled structure-acoustic modes   |
| $f_a$      | first air eigenfrequency                          |
| $f_b$      | first structural eigenfrequency                   |
| $f_H$      | Helmholtz resonance                               |
| $f_{m,n}$  | plate eigenfrequency                              |
| $f_s$      | fundamental frequency of the string               |
| $G$        | shear modulus                                     |
| $H_{sf}$   | spatial coupling matrix                           |
| $h$        | plate thickness                                   |
| $K_f$      | stiffness of the fluid                            |
| $K_s$      | stiffness of the structure                        |
| $L$        | string length                                     |
| $L_x, L_y$ | plate dimensions                                  |
| $l$        | length of the neck of the Helmholtz resonator     |
| $M_f$      | mass of the fluid                                 |
| $M_s$      | mass of the structure                             |
| $m, n$     | number of nodal lines in a specific dimension     |
| $N_{ij}$   | shape function                                    |
| $P_i$      | mechanical input power                            |
| $P_r$      | radiated sound power                              |
| $p$        | pressure  |
| $p_f$      | pressure of the fluid                             |
| $p_s$      | pressure of the structure                         |
| $Q$        | quality factor                                    |
| $r$        | radius of a sphere                                |
| $S$        | surface   |

|              |  |
|--------------|--|
| $s_{max}$    | maximum size of element                    |
| $T$          | string tension                             |
| $t$          | time                                       |
| $u_f$        | continuous displacement of the fluid       |
| $u$          | displacement (continuous)                  |
| $V$          | volume of the Helmholtz resonator          |
| $v$          | output velocity                            |
| $v_n$        | velocity amplitude at a single frequency   |
| $v_d$        | driving point velocity                     |
| $x, y, z$    | cartesian coordinates                      |
| $Y$          | mobility                                   |
| $Z$          | impedance                                  |
| $\alpha$     | isotropic loss factor                      |
| $\eta$       | power conversion efficiency                |
| $\mu_{ij}$   | Poisson ratio                              |
| $\rho$       | density                                    |
| $\rho_0$     | density of air                             |
| $\rho_s$     | structural density                         |
| $\sigma$     | averaged radiation efficiency              |
| $\sigma_n$   | radiation efficiency at a single frequency |
| $\sigma_s$   | structural stress                          |
| $\omega$     | eigenfrequency                             |
| $\mathbf{x}$ | vector $x$                                 |
| $\tilde{x}$  | complex variable $x$                       |

## Operators

|   |  |
|---|--|
| $d' = \partial_x d = \frac{\partial d}{\partial x}$ | partial derivate of $d$ with respect to $x$      |
| $\dot{d} = \frac{\partial d}{\partial t}$           | partial derivate of $d$ with respect to time $t$ |
| $\sum_\nu$  | sum over $\nu$                                   |
| $H^T$   | transpose of matrix $H$                          |
| $\tilde{\nabla}$                                    | modified gradient                                |
| $\nabla$  | gradient   |
| $\langle x \rangle$                                 | time average of $x$                              |
| $\bar{x}$   | spatial average of $x$                           |

## Abbreviations

|      |                                  |
|------|----------------------------------|
| BEM  | boundary element method          |
| CAD  | computer-aided design            |
| DOF  | degree of freedom                |
| FDM  | finite difference method         |
| FEM  | finite element method            |
| PML  | perfectly matched layer          |
| TMDF | tension modulation driving force |

# 1 Introduction

String instruments are based on a resonating body amplifying the string vibrations [1]. The body of the string instrument plays an important role in the sound radiation of the instrument as well as in its playability and quality [1, 2, 3, 4]. Understanding this role is important not only in gaining more understanding of the string instrument acoustics, but also for other purposes, such as sound synthesis [5], auralisation, and testing structural changes in instruments prior to building them [6].

Structural changes of the instrument body are of particular interest to luthiers, as they try to meet the requirements imposed by enlarging audience and concert halls [7]. This has led to the development of louder musical instruments, such as evolving a clavichord into a piano [1] and founding a new family of violins [8]. Similarly, in Finland a traditional string instrument called the kantele, that was originally used as a rune-accompaniment in small farm houses, is now played together with an orchestra in a large concert hall or with a band in a club. Consequently, the kantele has undergone many acoustic and structural changes from the 19th century onwards [9, 10].

The acoustics of the kantele string is well-researched while the body has had less attention. The acoustics of kantele was first analysed and synthesised by Karjalainen et al. [11] in 1993. The strong beating phenomenon was explained by the knotting of the strings. Later, in 2002, Erkut et al. [12] further studied and developed the synthesis of the kantele especially in relation to the physical mechanisms behind the characteristics of the kantele sound. The flexibility of the tuning pins turned out to cause some nonlinear behaviour in the kantele string. The nonlinearities were simulated by Pakarinen et al. [13] and Välimäki et al. [14]. As for the body, Peekna and Rossing [15] studied the vibration modes of six kanteles using electronic TV-holography. In addition, the modelling of vibrational modes of the top plate of a 40-string kantele has been reported [10]. The most recent work by Pölkki et al. [16] and Penttinen et al. [17, 18] has led to new construction rules for a modified kantele with increased loudness. Namely, the traditional kantele bodies are a closed box kantele and a top-plate kantele. The new modified body consists of a freely vibrating top plate separated from a back plate by an air gap.

String instrument bodies are complicated in geometry, material and boundary conditions. This leads to complicated partial differential equations governing the string instrument acoustics [1]. Solving these equations analytically is often impossible. To tackle this issue, several numerical methods have been developed to study string instrument acoustics with the attempt of modelling the acoustic behaviour as accurately as possible [5, 14, 19, 20, 21, 22, 23, 24, 25, 26, 27].

One of these physics-based numerical modelling methods is called the finite element method (FEM) developed in the 1960s [26, 28, 29]. It is based on approximating the continuous system with discrete elements, each following a set of equations. The method is widely used in acoustics [30, 31] and it has previously been applied to string instruments, such as violin [32, 33, 34, 35], guitar [36, 37, 38, 39, 40, 41, 42], and the piano soundboard [43, 44, 45, 46, 47]. FEM provides, for example, an interesting tool for studying structural and material changes of musical instruments

without building them.

This thesis extends the use of FEM to kanteles in attempt to understand the acoustics of the modified kantele body. It is an extension to the prior work by Pölkki et al [16] and Penttinen et al. [17, 18] on the development of a louder kantele. In their work, the modified kantele had also other improvements contributing to the increased loudness, such as extended top plate surface and higher string tension, whereas in this thesis the only variable is the size of the air gap. The aim is to understand how the vibrational and radiation characteristics of the modified kantele compare to the traditional top-plate kantele and box kantele. In addition, other structural changes in the modified kantele are briefly explored as a side-product of developing the FE-model. The FE-model is also compared to measurements. The main outcome of the thesis is the modified kantele combines free vibration of the top plate and the vibration of the enclosed air. This increases the number of modes and radiation efficiency of the modified kantele compared to the traditional kanteles.

This thesis is structured as follows. First, the acoustics and the construction of the kantele are briefly visited in Chapter 2. In Chapter 3, FEM is introduced. The focus is on the finite element formulation of a vibrational problem in the structure-acoustic domain. This is followed by review of the previous work done on applying FEM for string instrument acoustics. Chapter 4 presents the FE-model of the modified kantele and introduces the measurements that were made to verify the model. Chapter 5 presents the results of the modelling. Chapter 6 draws the results together and outlines some future work.

## 2 Construction and acoustics of the kantele

There are several instruments that are collectively referred to as *kantele* in Finland, *kannel* in Estonia, *kokles* in Latvia, *kankles* in Lithuania, and *gushli* in Russia. In these geographical areas the instrument is most commonly played [9]. Some of the kantele designs associated with different cultures and geographical areas are illustrated in Fig. 1. The design and the cultural history of the instrument varies from country to country. In Finland, the kantele has had a special function in the accompaniment of rune singing. Based on the transcripts of the runes, the estimates of the age of the kantele vary between 1000 and 3000 years [9, 10]. Similarly, there are many theories about the origin of the kantele. It is either originated from Asia, or Russia, or was separately invented by the ancient Finno-Ugric population [10].

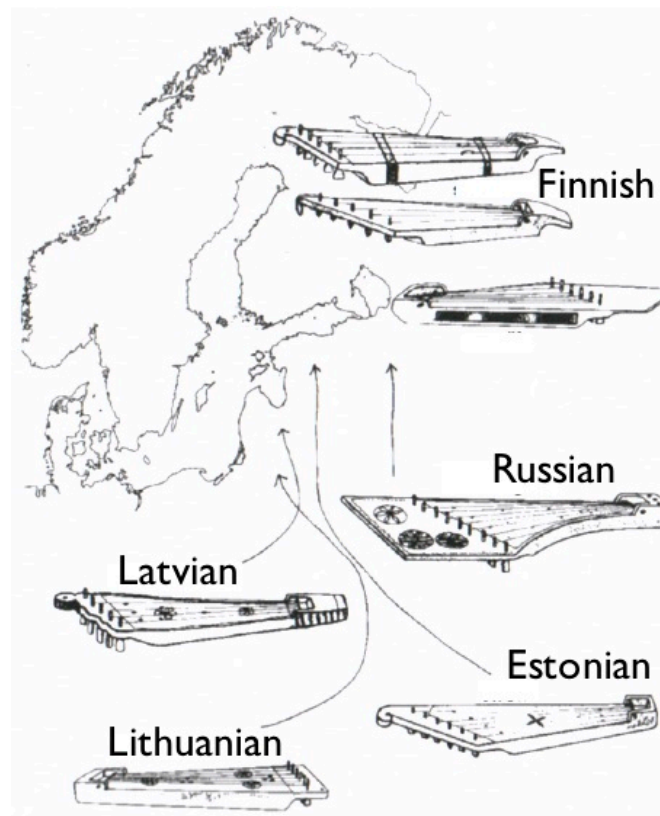


**Figure 1:** Some variations of the kantele in terms of geographical areas. Adapted from [9].

The common parts for all the kanteles include a wooden sound box (the body), metal strings, and tuning pins made of metal or wood. Initially, the kantele was carved from a single piece of wood. This method enabled only 5-9 strings in the body. After the introduction of wooden plates into the craft of kantele making in the 18th century, the amount of strings could be increased up to 40 [9]. In the 1920s, Paul Salminen developed a concert kantele which included a special lever system allowing rapid tuning of strings in order to enable chromatic playing [10].

Figure 2 illustrates the different kantele parts for a traditional Finnish five-string kantele. In addition to the body and strings, there is a horizontal steel bar called *varras* on the wooden extension, *ponsi*. The purpose of the *ponsi* is to allow the player’s arm to rest on it. The sound hole is typically a round hole, but not all kanteles have a sound hole. Finally, the strings are terminated on the individual tuning pegs or pins. In some kanteles, the *varras* is also replaced by individual tuning pins or pegs. One end of the string is wrapped around an individual tuning pin. The other end is knotted either to another tuning pin or around the *varras*, which connects all the strings together.

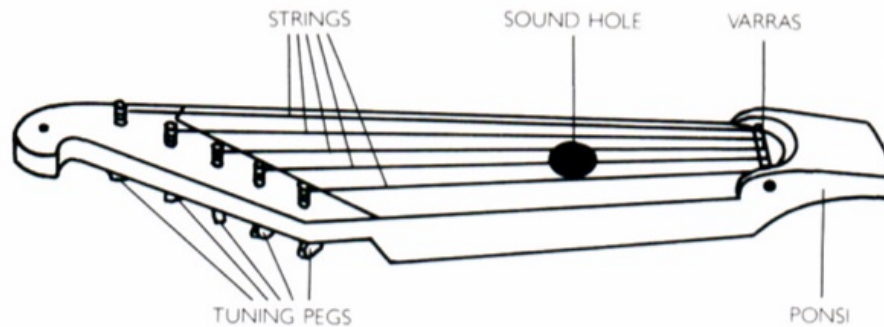


**Figure 2:** *The different parts of the five-string kantele. The tuning pegs are wooden, but in case they are made of metal, they are called tuning pins. Adopted from [48].*

The kantele strings are tuned diatonically with  $A = 442$  Hz. In diatonic tuning the scale is divided into seven whole tones and semitones [49]. The tuning of the modified 15-string kantele used in this thesis is from D2-D5 (73 - 588 Hz). The strings are usually plucked with fingers, but also nails, hammers, and plectra can be used. In addition to plucking, there is another playing technique which involves strumming the strings while damping some of them with fingers. Typically, the small kantele is held on lap with the shortest string facing the player, while the larger kanteles are played on a table.

The kantele, and the plucked string instruments in general, form a coupled vibrational system, starting from the string vibrations that excite the body via the string terminations. Finally, the vibrating body radiates sound in the air. Next, the acoustics of each part of the coupled system is discussed.

## 2.1 Strings

### 2.1.1 Ideal string vibration

When a string vibrates, it forms a standing wave pattern due to the reflections at the string terminations [1, 49]. Figure 3 shows the first three standing waves of the string in one dimension.  $N$  denotes the nodes of vibration, that is, the points that remain in place. These standing waves are the eigenmodes of the vibrating string. They are the modes at which the string vibrates naturally, i.e., when no driving force is applied on the string. The frequencies at which the eigenmodes occur are

called eigenfrequencies with the lowest eigenfrequency denoting the fundamental frequency. A steel string of length  $L$ , diameter  $d$ , density  $\rho$ , and tension  $T$  has the fundamental frequency  $f_s$  given by [1]

$$f_s = \frac{1}{L} \sqrt{\frac{T}{\pi \rho d^2}}. \quad (1)$$

In other words, the thicker, denser, or longer the string is, the lower its fundamental frequency. The more tightly it is set between the string terminations, the higher the fundamental frequency.

The higher eigenfrequencies are called string partials. In an ideal string, which is both harmonic and linear, the eigenfrequencies are in harmonic relationships to one another, meaning that the frequencies of string partials are integer multiples of the fundamental frequency. When a string is excited, the excitation of the partials is dependent on the excitation position. If the string is assumed to behave in a linear manner, the string plucked at  $\frac{1}{n}$  of its end will have the integer multiples of the  $n^{\text{th}}$  partial missing from its vibration [49]. What is more, under forced vibration, the excited modes are called resonances.

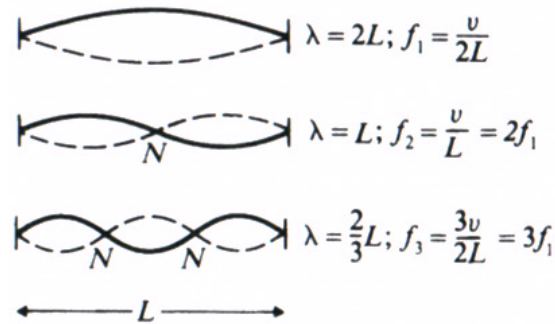


**Figure 3:** The first three standing waves or eigenmodes of a string.  $N$  denotes the nodes of vibration. Adopted from [49].

In reality the string vibrates in many dimensions. The standing waves pattern in Fig. 3 represents the transversal string vibration. In addition, the string vibrates in longitudinal and torsional dimensions that have their own eigenmodes. If the string is assumed to be linear, the three different type of waves are decoupled [50]. However, in the real string, the vibrational modes are combinations of these eigenmodes. Each of these waves have an importance in some musical instruments. For example, torsional waves are important in bowed string instruments [1]. Then again, the longitudinal waves are not that strong but they can have an audible effect, for example in the piano strings [51]. In the five-string kantele, the longitudinal waves can couple to the body because of the non-rigid tuning pins in the longitudinal direction [11, 12]. In general, the transversal waves are the most important when it comes to plucked string instruments.

What is more, the transversal waves in the string are polarised, meaning that the string vibrates in two different transversal planes; horisontal and vertical [1].

The way the strings are terminated to the body typically induces different effective lengths for the string in each polarisation direction. This gives rise to two slightly differing fundamental frequencies in the string, leading to a periodic change in the amplitude of the string vibration, i.e., beating.

In the five-string kantele, the two different effective lengths arise from the knotting of the strings to the varras [11], as illustrated in Fig. 4. The vertical polarisation is directed up and down the page while the horizontal polarisation occurs in and out of the page. For the vertical polarisation, the knot is the termination point for the string. For the horizontal polarisation, the contact point of the string with the varras is the termination point.  $\Delta l$  denotes the difference in length.

The same knotting is used in the modified kantele, but instead of the varras, both ends are terminated on tuning pins. Figure 5 shows the decay of the first three harmonics of the highest string in the modified kantele, when plucked in the middle. The beating of the harmonics can be observed in the envelope trajectories.

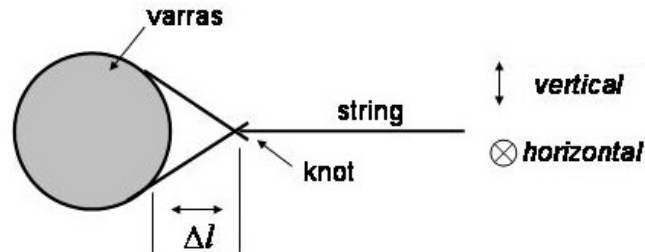


**Figure 4:** *The two different effective lengths of the kantele string induced by the string knotting. The horizontal vibrations are directed up and down the page whereas the vertical vibrations in and out of the page. The length difference is assigned with  $\Delta l$ . Adapted from [11].*

### 2.1.2 Real string vibration

The actual string vibration is nonlinear and inharmonic [50]. For example, in the five string kantele, the second harmonic of the string has been found present, even though the string was plucked in the middle [12]. It is also detected for the modified kantele, as it can be seen in Fig. 5.

The nonlinearity in the real string arises from many factors. Firstly, there is the pluck. When a string is plucked, its length changes. The change in the string length introduces a change in its tension. Finally, the change in string tension changes the fundamental frequency of the string. This tension modulation is the major contributor to the nonlinear behaviour of the string [52]. Especially in the kantele, there is an audible frequency decent after the pluck, because the string tension decreases. This frequency decent can be used to extract more information about the nonlinear behaviour of kantele strings [12].

The second cause for nonlinearity is the non-rigid string terminations. In many other string instruments, the string termination, such as the bridge, does not effec-

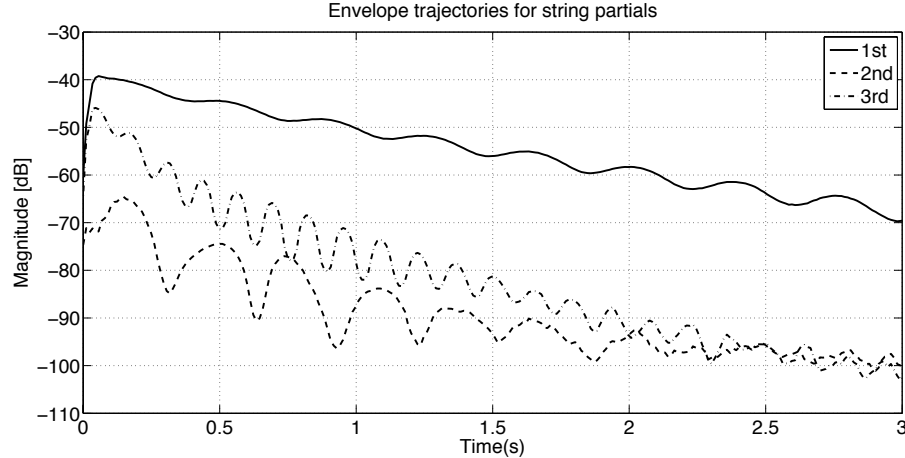


**Figure 5:** *The envelope trajectories of the first three harmonics of the highest string ( $f_0 = 589$  Hz) of the 15-string modified kantele, when plucked in the middle of the string. The solid line represents the first harmonic, or the fundamental frequency, the dashed line is the second harmonic, and the dash-dotted line represents the third harmonic.*

tively transmit the longitudinal vibrations of the strings. However, in the kantele, the tuning pins are not rigid in the longitudinal direction. Together with the tension modulation, the non-rigid tuning pins create a longitudinal force component in the vibrations, called the tension modulation driving force (TMDF) [12, 13]. In the case of the 5-string kantele, TMDF is responsible for another characteristic feature of the kantele sound, the high initial amplitude of the second harmonic [12]. Interestingly enough, the high initial amplitude of the second harmonic cannot be observed in the modified kantele on the basis of Fig. 5.

The inharmonicity in real string stems from dispersion, i.e., different frequency components in the string travel at different velocities. The two main sources for dispersion are the finite string stiffness and the damping mechanisms [1]. Finite stiffness in strings raises the upper partials, and thus they are no longer in harmonic relationships with the fundamental frequency. This phenomenon is particularly important in the tuning of piano strings. The main damping mechanisms of string vibration are air viscosity, viscosity of the string material, and the energy loss through the tuning pins/bridge to the body [1]. For thin metal strings, such as the kantele strings, the most dominant damping mechanism is the air viscosity.

## 2.2 Body

### 2.2.1 Structure

There are two prevailing structures of the kantele body, namely the top-plate kantele and the box kantele. The top-plate kantele has no back plate, i.e., the body is open, as shown in Fig. 6. The box kantele has a completely closed body, such as the kantele presented in Fig. 2. Both structures may or may not have sound holes.

In addition to these two traditional structures, there exists a kantele with sep-



**Figure 6:** A few examples of top plate kanteles.

arate top and back plates, as illustrated in Fig. 7. It is called a modified kantele. A separate back plate has been added to the top plate so that there is an air gap between the two plates. A typical size of the air gap is 5-6 mm. The two plates are connected together with three plastic screws as indicated in Fig. 7. In addition, a sound hole is formed by the curved ribs of the top and the back plates. Some bars are also attached to the top and the back plates in order to make them stiffer. These bars can be seen in Fig. 8 which illustrates the inside of the modified kantele.

In the modified kantele, the top plate acts as a free-edge vibrator. In particular, the tuning pin edge of the kantele is able to vibrate freely, because the side has been removed. The modified structure was designed bearing in mind that the kantele is typically played on the lap. When held on lap, the sides of the kantele are damped. In the modified kantele, because of the air gap, the top plate vibrates freely even if the back plate is damped on the lap [17]. In addition, the back plate enclosed air that contributes to the plate vibrations. The modified kantele has been proven to be louder than the top plate kantele [17]. It should be noted that this special structure resembles the resonator added to the banjo [53] and the floating top plate of the hammered dulcimer [54].

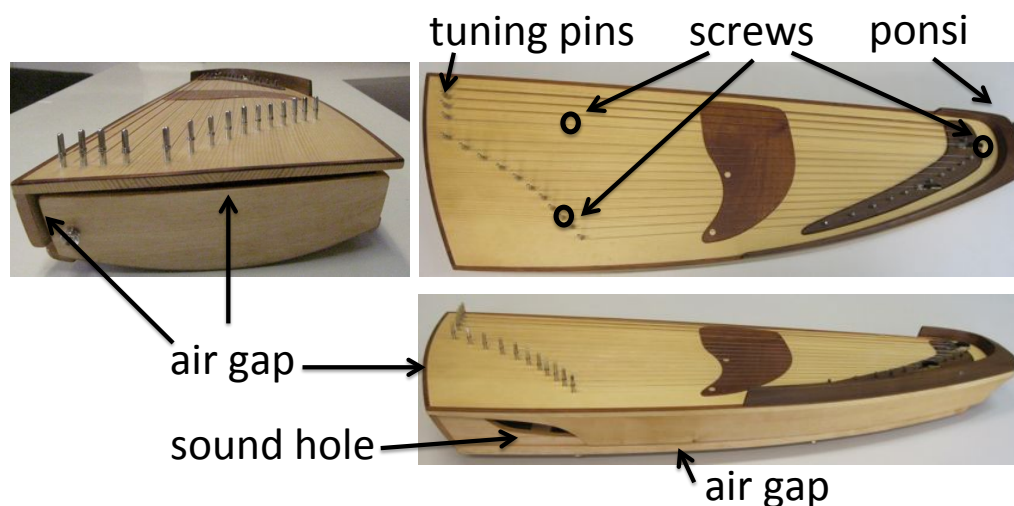


**Figure 7:** The modified kantele with the air gaps indicated.

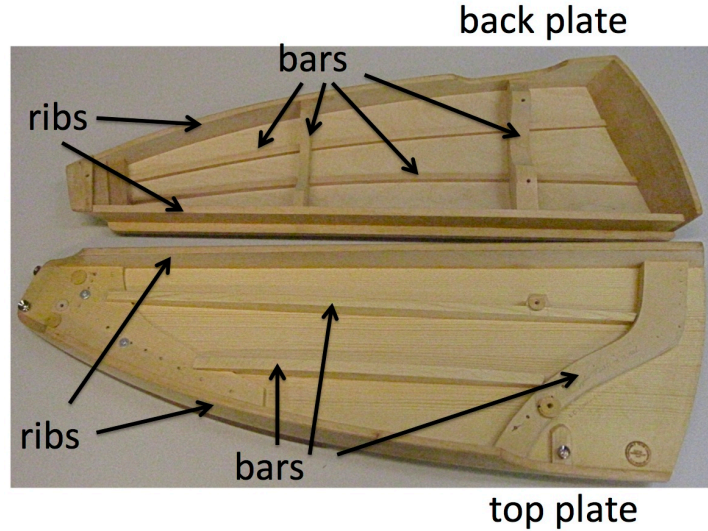


**Figure 8:** *The modified kantele with the bars, ribs, and plates indicated.*

### 2.2.2 Materials

The most common materials for the kantele body are pine (*Pinus sylvestris*) and spruce (*Picea abies*) [9]. Some more exotic species are used in decoration and in strengthening the top plate under the tuning pins. As an example, the wood species used in the modified kantele are listed in Tab. 1. In general, different wood materials have different properties such as internal damping, density, and stiffness, which make them suitable for different parts and types of string instruments [55, 56]. One way for an instrument builder to affect the sound of the instrument is by the selection of material for the body.

| Species  | Parts of the kantele                        |
|--|---|
| Spruce ( <i>Picea abies</i> )                      | top plate, top plate ribs, top plate braces |
| African walnut ( <i>Lovoa trichilioides</i> )      | ponsi, top plate decorative coating         |
| Grey alder ( <i>Alnus incana</i> )                 | back plate ribs, back plate braces          |
| Honduras mahogany ( <i>Swietenia macrophylla</i> ) | top plate coating                           |
| Birch plywood                                      | back plate, brace under the tuning pins     |
| Norway maple ( <i>Acer platanoides</i> )           | braces by the three screws                  |

**Table 1:** *Wood species used for the modified kantele.*

Wood is considered to be an orthotropic material due to its cellular structure [56, 57]. In other words, its material properties differ in three mutually perpendicular axes: radial (R), tangential (T), and longitudinal (L). The R-axis is defined perpendicular to growth rings, the L-axis parallel to the fibre, and the T-axis perpendicular to fibre but tangent to growth rings. These axes are illustrated in Fig. 9. The figure also shows how the wooden plates of a musical instrument, such as the

violin, are typically cut (called quarter-cut). In this case, the T-axis is in the direction of the thickness of the plate, and the R-and L-axes form the transversal plane of the plate. The plates of the modified kantele are also cut like this.

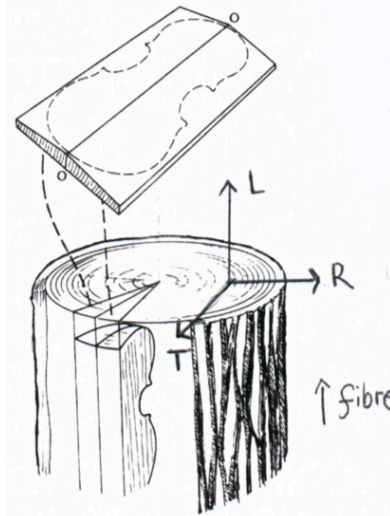


**Figure 9:** *The perpendicular axis of wood labelled with L for longitudinal, R for radial, and T for tangential. The wooden plates for a violin, as well as for the kantele, are cut so that the tangential axis is in the direction of the thickness of the plate, and the radial and longitudinal axis form the plane of the plate. Adapted from [49]*

All in all, twelve constants are needed to describe the vibrational characteristics of wood: three elastic moduli (Young's moduli), three shear moduli, and six Poisson's ratios [58]. Nine of these are independent, since the elastic moduli  $E$  and Poisson's ratios  $\mu$  are related according to

$$\frac{\mu_{ij}}{E_i} = \frac{\mu_{ji}}{E_j}, \quad i \neq j, \quad i, j = L, R, T. \quad (2)$$

The constants defining the acoustical properties of wood are primarily density, elastic moduli, and loss factor [56]. Density  $\rho$  and Young's moduli  $E$  define the speed of sound in wood  $c$

$$c_i = \sqrt{\frac{E_i}{\rho}}, \quad i = L, R, T. \quad (3)$$

In wood, the Young's modulus varies with direction and thus also the speed of sound is different. For example, the tangential speed is around one-fourth of that of the longitudinal. Typical longitudinal speed of sound for wood material is between  $3000\text{-}7000 \text{ ms}^{-1}$ .

The loss factor measures the dissipation of vibrational energy due to internal friction in the material. Internal friction depends of the moisture content and temperature [58]. The value for the loss factor for wood is between  $\alpha = 0.002 - 0.1$  [56, 58].

### 2.2.3 Plate vibration

Similarly to the string vibration, the vibration of an instrument body consists of several different types of standing waves, or eigenmodes. In a finite thin plate, such as the kantele top plate, there exist transversal, longitudinal, quasi-longitudinal, flexural (or bending), torsional, and surface waves [59]. The deformation patterns of some of these wave types are shown in Fig. 10. Of these, the flexural waves, shown in Fig. 10c, couple well with air and are important in sound radiation. This is because the flexural waves involve relatively large displacements normal to the direction of propagation and can thus effectively displace the air [59, 60]. However, when the wavelength of the flexural waves becomes comparable to the thickness of the plate, the vibrations of the plate become more complicated. In addition, at the boundaries and at the point of excitation of the finite plate, all the mentioned types of waves can couple with each other [59, 60]. In other words, one wave type can excite any of the other at these points.

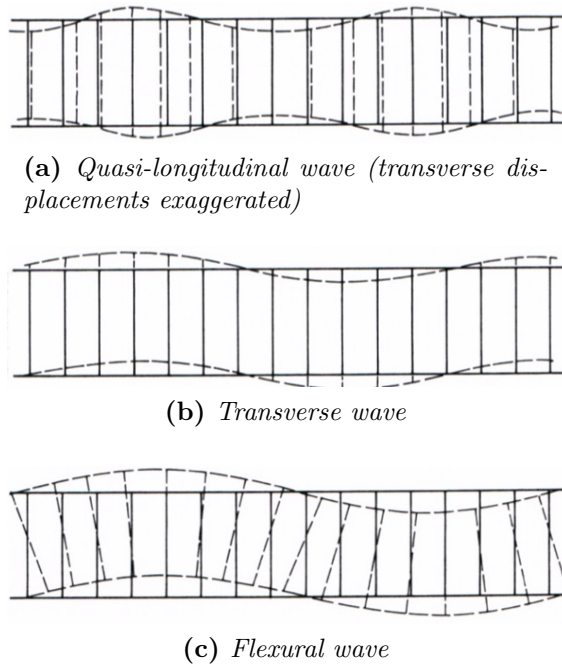


**Figure 10:** *Deformation patterns for some of the wave types in a plate. Adopted from [60]*

It is worth noting that the speed of the flexural waves in a plate is dispersive, i.e. the speed depends on the frequency. For a homogenous plate, the speed of the flexural waves  $v(f)$  is [1]

$$v(f) = \sqrt{1.8fhc_L}, \quad (4)$$

where  $h$  is the plate thickness and  $c_L$  the speed of sound in the longitudinal direction. The dispersion is more complicated for orthotropic plates in the presence of fluid loading, such as the case of musical instrument plates [61].

In the kantele, the eigenmodes and their frequencies depend on the geometry of the top and the back plate, and how they are attached to another. Usually, the

plates are fixed to another by the ribs. In the case of the modified kantele, the top plate is resting on the back plate and can be considered simply supported on the location of the three screws. Since the instrument plates are typically rather thin, around 5 mm for the kantele for example, the eigenmodes can be studied in two dimensions. For a simply supported, orthotropic rectangular plate with dimensions of  $L_x$  and  $L_y$  and thickness  $h$ , the eigenfrequencies of the flexural waves are given by [1]

$$f_{m,n} = 0.453h \left[ c_x \left( \frac{m+1}{L_x} \right)^2 + c_y \left( \frac{n+1}{L_y} \right)^2 \right], \quad (5)$$

where  $m$  and  $n$  are the amount of nodal lines the vertical and horizontal directions, respectively, and  $c_{x,y}$  is speed of sound in the material in the respective direction. The eigenmodes of the plates are labelled according to the nodal lines in each dimension. When the plate is fixed, the shape  $(0,0)$  is the first eigenmode with the lowest frequency and no nodal lines present [1]. The shape  $(1,0)$  has one nodal line in the longest dimension, and this is also the first eigenmode for a freely vibrating plate. It is worth noting, that instrument plates have typically more complicated form than a rectangle and have changes in the plate thickness. Also, the boundary conditions are not necessary simple. This is where the need for physical modelling stems from.

It is possible to make some general remarks based on Eq. 5. First of all, unlike the ideal string eigenfrequencies, the plate eigenfrequencies are not harmonic. This is in fact the case with the body modes of most of the wooden string instruments [1]. Secondly, if lower eigenfrequencies are desired, the plate can be thinned, or the plate area enlarged.

The normal modes of the plates depend on the excitation. Namely, the closer the plate is excited to location of an antinode, the more easily the corresponding eigenmode is excited [1]. In other words, if the excitation point is very near to a node, then the corresponding eigenmode will not be excited.

Musical instrument bodies are typically assumed to be linear [25], which means that the eigenmodes and the eigenfrequencies are not depended on the amplitude of the vibration. Another implication of the linearity is that when the body is excited, say sinusoidally for example, the observed vibrational modes are no longer necessarily eigenmodes, but combinations of them [62]. An example of the coupling of two eigenmodes  $(2,0)$  and  $(0,2)$  for rectangular quarter-cut spruce plates is shown in Fig. 11 for different degrees of coupling. The left-hand side describes the situation when  $(0,2)$  is more dominant and the right-hand column when  $(2,0)$  is more dominant. The difference between the top row and the bottom row is opposite signs in amplitude. Full coupling of the two modes occurs on the third row of Fig. 11 .

Combinations of modes that occur with forced excitation are called operation deflection surfaces (or more commonly resonances). They are typically combinations of modes that are close to or within the frequency range of the excitation [60]. These vibrational modes typically are well-separated in frequency at low frequencies. However, at high frequencies their density increases and it become more difficult to distinguish the individual modes from one another.

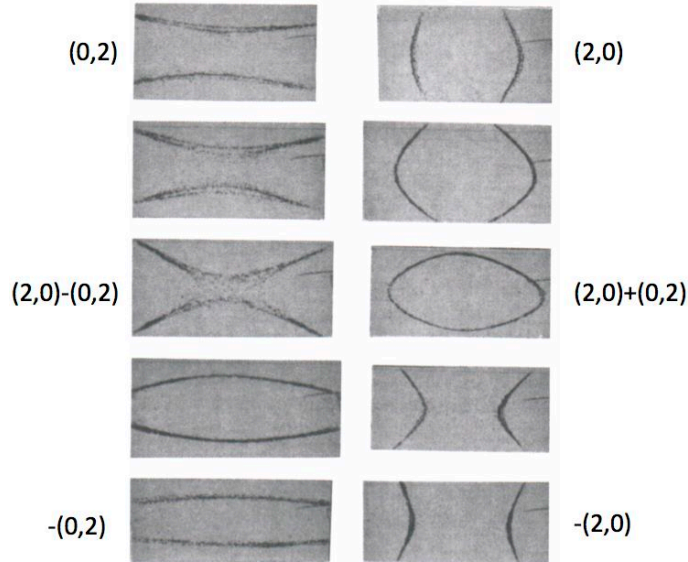


**Figure 11:** *Coupling of two eigenmodes  $(2,0)$  and  $(0,2)$  for rectangular quarter-cut spruce plates with different degrees of coupling. The left-hand side describes the situation when  $(0,2)$  is more dominant and the right-hand column when  $(2,0)$  is more dominant. The difference between the top row and the bottom row is opposite signs in amplitude. Full coupling of the two modes occurs on the third row. Adapted from [1].*

### 2.3 Coupling between the strings and the body

When a string is set to vibrate, the vibrations are transmitted to the instrument body, in the case of the kantele via the tuning pins. The coupling between the strings and the body is commonly described through mechanical impedance. It is the measure of how much a structure resists motion with a given force. It is defined as the ratio between the input force  $F$  and the output velocity  $v$  in the frequency domain. The reciprocal of the mechanical impedance is the admittance or mobility  $Y$ . Mathematically, the impedance  $Z$ , as a complex variable, can be expressed in frequency domain as follows [1]

$$\tilde{Z}(\omega) = \frac{1}{\tilde{Y}(\omega)} = \frac{\tilde{F}(\omega)}{\tilde{v}(\omega)} \quad (6)$$

Typically, the impedance of the string is at least an order of ten lower than that of the string termination [1]. This impedance mismatch enables strong reflections of the string vibrations at the termination points which, in turn, create the standing waves on the string. The decay rate of the string vibrations depends on this impedance mismatch, as well. As a matter of fact, the decay of the string vibrations has typically two stages because of the different impedances of the string termination in the vertical and horizontal directions [63]. At first, the decay is rapid, but after some tens of milliseconds, the decay rate decreases.

In general, the energy of the vibrating string is absorbed slowly by the body. At the vibrational modes of the body, however, the vibrational energy is better transmitted to the body. At these frequencies, the impedance of the body is reduced.

In this case, it can also happen that the string reflections are too weak to sustain the standing waves. An example of this kind of a strong coupling between the body and strings is the wolf-tone in bowed instruments [1, 64]. The bowed string releases its energy to the body quickly and the string vibration dies out. At the same time, the body vibrations run out of their energy source and a new energy cycle is ready to begin. The outcome is that the string and the body vibrations alternative in amplitude, which hardly results in a steady tone. Indeed, the coupling between the string and the body is always a question of balance between a sustained tone or a loud tone. For example, thinner plates in the instrument body tend to radiate more sound power, but the string vibrations decay quickly [23].

Since the body amplifies the string vibrations, the closer the vibrational modes of the body are to those of the string, the better these body resonances are excited. The vibrational modes of several different kantele bodies have been investigated by using electronic TV holography by Peekna et al. [15]. They have suggested that the more vibrational modes there are with the tuning range of the kantele, the better the kantele is in terms of sound quality and level.

The body also acts as a transmitter of energy between the strings. When one string is played, the other strings can also contribute to the musical sound via the body. This phenomenon is called sympathetic vibration. For the kantele, it can be considered an important phenomenon, as the other strings are not damped when one of them is plucked. In the case of the kantele, it has been found out that the sympathetic vibrations are most pronounced between strings with simple harmonic relations [12]. The analytical treatment of sympathetic string vibration has been focusing on instruments with a bridge [1, 65].

## 2.4 Coupling between the body and the enclosed air

Apart from the mechanical vibrations, the kantele body encloses some air that vibrates and has its own eigenmodes. Unlike solids, the air can only support one type of waves, the longitudinal waves. The enclosed air also exerts a load on the body, thus affecting the eigenfrequencies of the body [35]. In turn, the shapes of the eigenmodes of the body remain almost unchanged. In the case of sound hole, the fundamental eigenmode of the air is called the Helmholtz resonance. This means that the mass of the air at the sound hole acts as piston and the air inside the body as a spring. The frequency of the Helmholtz resonance is given by [1]

$$f_H = \frac{c_0}{2\pi} \sqrt{\frac{A}{Vl}}, \quad (7)$$

where  $c_0$  is the speed of sound,  $A$  is the area of the sound hole,  $V$  is the volume of the resonator, and  $l$  is the length of the sound hole. The other eigenmodes of the air inside a box resemble standing waves in a rectangular box [49, 62].

When the lowest structural and air modes couple, the coupled modes follow the rule [66]

$$f_b^2 + f_a^2 = f_1^2 + f_2^2 \quad (8)$$

where  $f_b$  is the lowest structural eigenfrequency of the top plate,  $f_a$  the lowest eigenfrequency of the enclosed air, and  $f_1, f_2$  are the lowest frequencies of the coupled system.

## 2.5 Coupling between the body and the surrounding air

The vibrations of the strings and the body couple with the surrounding air according to how effectively they can displace air. The coupling depends on the level and frequency of the vibration, the shape of the body, the spatial distribution of the surface motion, and of course the properties of the air. Sound consists of longitudinal compression waves in the air. Thus, the larger displacements the mechanical vibrations can cause, the better the vibrations will radiate in air. To be more precise, the particle velocity normal to the surface of the plate is the same as the particle velocity of the air [60].

The string vibrations on their own couple poorly with air because the string acts as a dipole source with a small radius [1]. Thus, the compressions and rarefactions of air it creates effectively cancel each other. On the contrary, the vibrations of the body, in particular the flexural waves of the plates as described earlier, involve greater displacements of air. At low frequencies, the sound is mostly radiated by the top plate, the back plate and the sound hole [49]. At high frequencies, the top plate is the main source of radiation.

### 2.5.1 Radiated sound power

The total radiated sound power of a source is defined as the integral of the sound intensity vector over the closed surface around the source [67]. Under anechoic conditions so that the radiated sound is approximated with a plane wave, the total radiated sound power is defined as the integral of the pressure squared over the surface  $S$

$$P_r = \frac{1}{\rho_0 c_0} \int_S p^2(S) dS, \quad (9)$$

where  $\rho_0$  is the density of air, and  $c$  is the speed of sound in air.

At discrete measurement points  $n$ , distributed uniformly over the surface of a sphere, Eq. 9 becomes

$$P_r = \frac{4\pi r^2}{\rho_0 c_0} \frac{1}{n} \sum p_n^2, \quad (10)$$

which means that the total radiated sound pressure is the mean square average of the pressure multiplied by the area of the sphere divided by the characteristic impedance  $Z = \rho_0 c_0$  of the air.

There are many ways to choose the measurement points of the surface of the sphere. The only requirement is that the points are uniformly distributed in order to use the simplified expression (Eq. 10). Examples of this kind of spatial sampling methods are interpolation, weighted quadrature (e.g., platonic solids), least-squares transforms and triangulated meshing [68]. In practice, the radiated sound power is

often measured on a hemisphere. For this case, there is an ISO standard for selecting the measurement points, 10 altogether [67].

### 2.5.2 Radiation efficiency

Radiation efficiency is defined by a reference to a baffled piston vibrating uniformly at frequencies for which the piston circumference clearly exceeds the acoustic wavelength [60]. Radiation efficiency can be more than one, but in most practical cases it is below or close to unity. It is defined as

$$\sigma_n(f) = \frac{P_r}{\rho_0 c_0 S_v \overline{\langle v_n^2 \rangle}}, \quad (11)$$

where  $S_v$  is the area of the vibrating surface, and  $\overline{\langle v_n^2 \rangle}$  is the average mean square velocity at a certain frequency, meaning that it is the squared vibration velocity averaged in both time and space. The radiation efficiency here is defined for an individual mode  $n$ .

Radiation efficiency of the individual modes weighted with the corresponding velocity amplitudes gives the average radiation efficiency over a frequency range [59]

$$\sigma = \frac{\sum_n \sigma_n(f) \overline{\langle v_n^2 \rangle}}{\sum_n \overline{\langle v_n^2 \rangle}}. \quad (12)$$

### 2.5.3 Cancellation of radiation

Because the speed of flexural waves is dispersive, it can either be smaller, equal, or greater than the speed of sound in air. Sound radiation and radiation efficiency depend on the relationship between the structural and the acoustic wavelength.

The frequency at which these two wavelengths are equal is called the critical frequency. For example, for wood there exists a critical frequency for each orthotropic direction. For the guitar, they are estimated to be around  $f_{cL} = 1$  kHz along the fibre and around  $f_{cT} = 2$  kHz across fibre [41]. For violins, the values are  $f_{cL} = 0.5$  kHz and  $f_{cT} = 1.8$  kHz [1]. Naturally, this depends on the thickness of the plates (see Eq. 4).

Above and below its critical frequency, the plate behaves very differently in terms of radiation. Above the critical frequency, or when the flexural wavelength is greater than the acoustic wavelength, the radiation efficiency is always unity or above [59, 60]. The plate is said to act as a surface radiator.

Below the critical frequency, there is no radiation for infinite plates [59, 60]. For finite plates, the radiation efficiency is significantly lower than unity. This is because of hydrodynamic short circuit. Two adjacent regions vibrating in opposite phases can cause radiation cancellation, such as the case of the string, or an unbaffled bass loudspeaker. This cancellation occurs when the regions are much less than half a wavelength apart [60].

This cancellation at subcritical frequencies in finite plates means that they become either edge or corner radiators. If the flexural wavelength in one dimension is

smaller than the acoustic wavelength, the plate radiates only at its edges depending on which dimension the wavelength is smaller. If the flexural wavelength is smaller in both dimensions, then the plate radiates at its corners. These edge and corner modes are shown in Fig. 12.

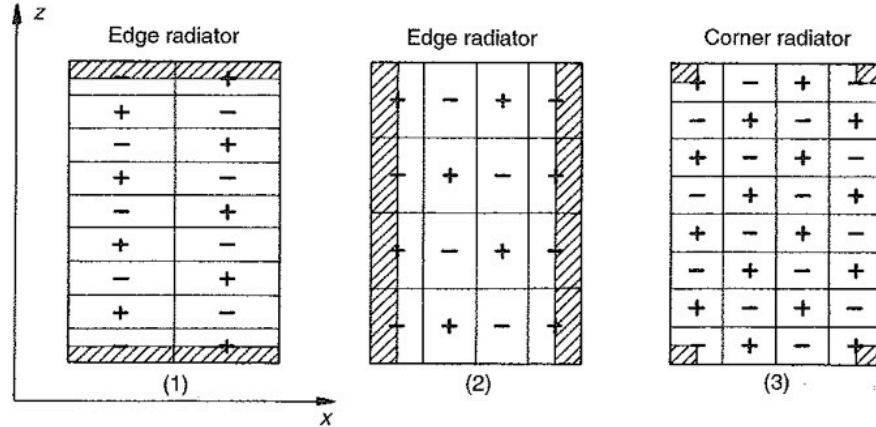


**Figure 12:** Three cases of edge and corner radiators with antiphase regions indicated. The crossed area is radiating to the air. Adopted from [60].

The critical frequency plays a role in musical instruments. It has been proposed for example that violins that are considered to have a good sound quality have low critical frequencies [69]. Namely, thicker violin plates have lower critical frequencies. Furthermore, the radiation efficiency of modes at subcritical frequencies (edge and corner modes) have been studied on the guitar using FEM by Torres et al. [41]. The guitar edge modes radiate more efficiently than corner modes as well as modes with odd symmetries of antiphase regions radiate better than those with even symmetries.

#### 2.5.4 Power conversion efficiency

Another measure related to sound radiation is the power conversion efficiency  $\eta$  which is defined as the ratio between the total radiated sound power  $P_r$  and the mechanical input power  $P_i$  [59, 70], that is

$$\eta(f) = \frac{P_r(f)}{P_i(f)}. \quad (13)$$

The mechanical input power is defined as the complex scalar product of the force and the velocity amplitude at the driving point,  $F_d$  and  $v_d$ , respectively, [70]

$$P_i(f) = \Re \{ F_d v_d(f)^* \}. \quad (14)$$

Consequently, power conversion efficiency depends on the excitation: on its location and force. Typical radiation efficiency of a musical instrument has the order of magnitude of 0.01 (or 1%) when excited artificially [41, 70]. Estimation of radiation efficiency while playing is difficult because of the difficulty to measure player's mechanical input.

### 2.5.5 Directivity

Sound radiation of a musical instrument depends on direction, because the instrument body enables a complex directivity pattern [25]. Directivity is the measure of how much of the total energy is radiated in a certain direction. Directivity depends also on frequency and on the excitation [1]. In a normal room the directivity pattern is obscured by the reflections of the sound. An example of a measured directivity of the modified kantele using coarse dodecahedron spatial sampling [71] is presented in Fig. 13.

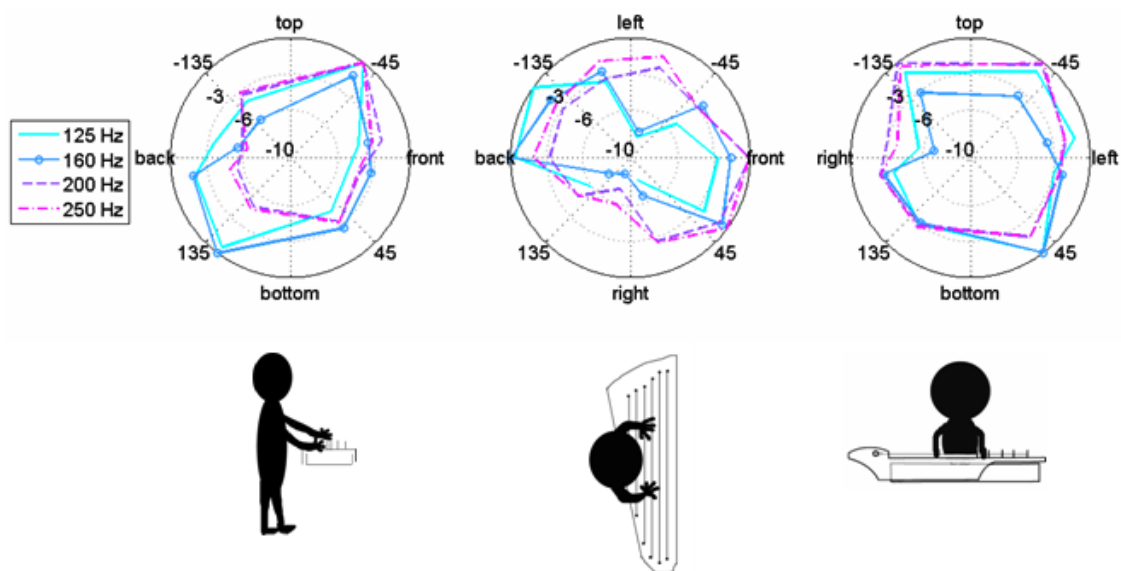


**Figure 13:** Directivity of the modified kantele at selected third-octave bands when all strings are excited. Under each polar plot, the positioning of the instrument and the player at the centre of the plot is depicted.

### 3 Finite element method in string instrument modelling

Acoustic problems are governed by partial differential equations with complicated boundary conditions [28, 31, 59, 60, 72, 73]. It is often impossible to solve the equations analytically. Therefore, numerical methods have been developed to solve these problems approximately. These numerical methods include among others finite difference, boundary element, and finite element methods [19, 28, 29, 31, 74, 75]. The differences of these methods lay in the formulation of the partial differential equations describing the problem. In general, the partial differential equation domains are divided into elements following certain functions specific to the method. The finite difference method (FDM) is based on the differential formulation of the problem. In this method, the solution domain is divided into a grid. FDM works well for less complicated structures, such as bars and plates, especially in one or two dimensions.

The boundary element method (BEM) is, in turn, based on the integral equation formulation of the problem. As the name suggests, only the boundaries of the domains are treated and they are divided into surface elements. BEM is suitable for modelling the sound radiation of the instrument or the behaviour of the air enclosed by the instrument [75]. If the instrument has structural modes in the same frequency region as the acoustic modes, then finite element approach is required [31].

Finally, the finite element method (FEM) is based on the weak formulation of the problem. Weak formulation means that the continuity of the partial differential equations is weakened so that the equations hold only for a certain set of functions. In FEM, the entire domain is divided into solid elements [28]. There are two different approaches to FEM: variational and weighted residuals [31]. The variational approach is based on the minimum energy principle while the residual method is based on minimising the error between the approximate and the analytic solution. There are actually several specific weighted residual methods, such as the Least Square method and the Galerkin method [28, 29, 31, 76]. Further reading on the residual methods can be found for example in [76].

All these methods are used in string instrument modelling since it is often beneficial to study the interaction between each constitutive part of the musical instrument separately, instead of trying to complete a model of the whole instrument [27]. A typical way of modelling a string instrument starts with modelling the vibrational modes of the instrument body with FEM [23, 26, 33, 34, 35, 36, 38, 39, 40, 41, 42, 43, 44, 45, 46, 47] or FDM [19, 77, 78]. Then, the body vibrations are coupled with a string model using, e.g., FDM. Finally, the radiation of the whole instrument is calculated using BEM. The validity of the simulation is often checked with measurements.

FEM is most suited for modelling both the vibrational modes of the instrument and its sound radiation because the entire domain is approximated with solid elements [31]. Indeed, string instruments are essentially wooden boxes vibrating in air, i.e., coupled structure-acoustic systems. Hence, the finite element formulation pre-

sented in this chapter focuses on the coupling of these two domain. The variational formulation of FEM is used. After the theoretical basis, previous work on string instrument modelling with FEM is reviewed.

### 3.1 The basis of finite element method

The basic idea of FEM is that a continuous, complicated system can be divided into smaller subsystems whose behaviour can be simplified and approximated [28, 29, 72, 74]. This process is known as *discretisation*. These subsystems, more commonly known as elements, are connected to one another via nodal points at the boundary of each element. It is then the displacements of the nodal points that are the unknown parameters of the system, instead of the infinitely many unknown displacements of a continuous system. In other words, the end result is discrete unknowns approximating an unknown continuous field. This implies that the amount of nodal points equals the degrees of freedom (DOFs) of the discretised system.

The connection between the continuous field  $u(x, y, z)$  and the nodal points  $d_j$  is established through *shape functions*  $N_{ij}(x, y, z)$ , so that

$$u(x, y, z) = \sum_j N_{ij}(x, y, z)d_j. \quad (15)$$

The shape functions approximate the behaviour of the elements between the nodal points. The shape functions are required to be piecewise differentiable and continuous at the boundaries connecting two elements [31]. Most often, the shape functions are polynomials fulfilling these requirements.

A simple example of the selection of the shape functions is illustrated in Fig. 14 adapted from Ottosen et al.[29]. The temperature is first represented as a one-dimensional continuous field quantity (Fig. 14a). Next, the temperature function is discretised, i.e., divided into elements (line segments) and nodal points (Fig. 14b). First, the elements are approximated with a first-order shape functions (Fig.14c) and then with the second-order shape functions (Fig. 14d).

The process of discretising the geometry of the system with elements is called *meshing*. The selection of element type and shape used for the meshing depends on the dimensions of the system. The element types include solids, shells, and beams, among others. Solid elements are three dimensional, i.e., with three variables approximating the field at each nodal point. In shell elements one of the dimension has been collapsed because it is relatively small to the other two. Further, in beam elements, two of the dimensions are collapsed. For shell and beam element models, there are two and one variables describing the field, respectively. As for the shapes, in two dimensions, triangles and quadrilaterals are typical. In three dimensions, the elements are typically tetrahedral or cubic. In the same model, it is possible to use more than one element type, but then the compatibility between the different elements must be forced when meshing.

In addition to the shape functions, the system behaviour is governed by the *boundary conditions* of the system. Otherwise, the partial differential equations would not have unique solutions. The boundary conditions can be divided into two

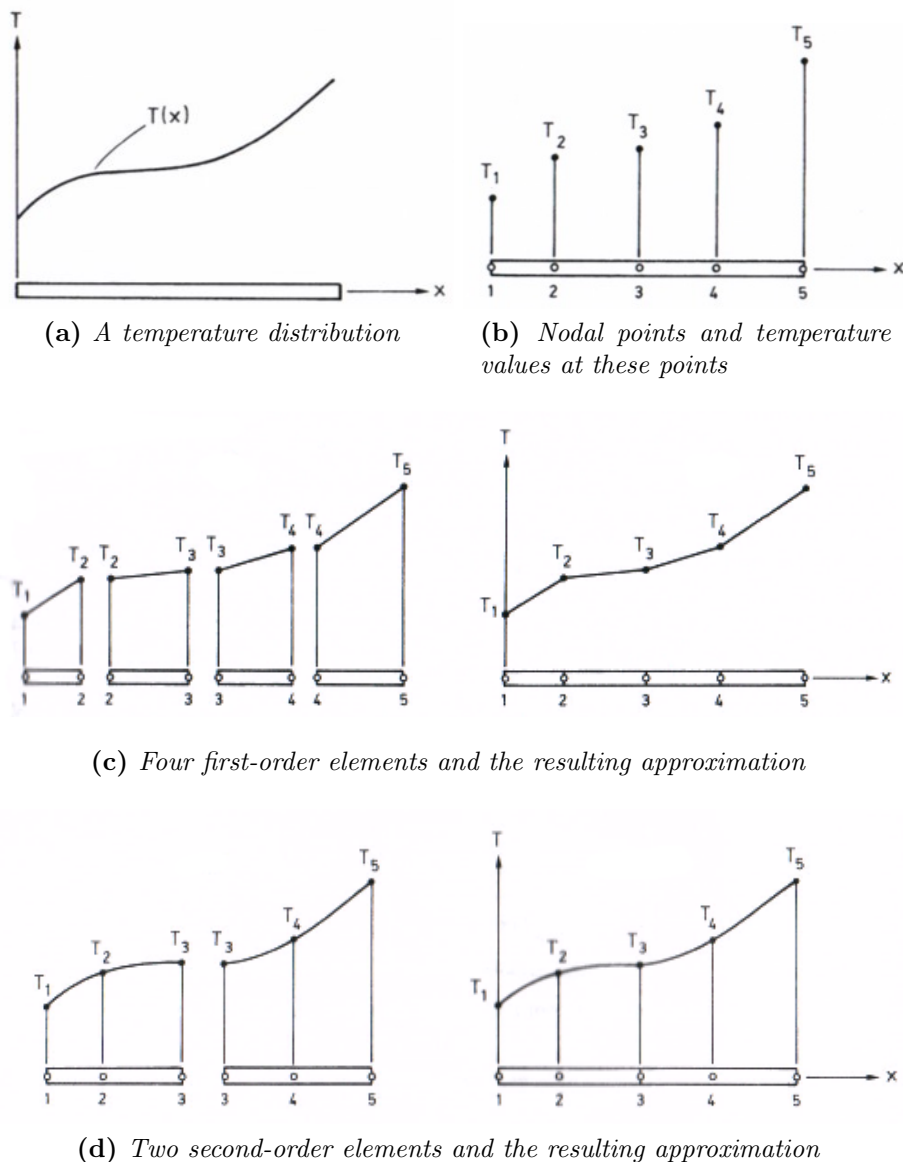


**Figure 14:** Discretising a one-dimensional temperature distribution with first- and second-order elements. Adapted from [29]

categories: natural and essential. The difference between the two is that natural boundary conditions do not eliminate any degrees of freedom. Natural boundary conditions arise in the process of solving the partial differential equation, such as the boundary conditions between structural and acoustic domains. On the contrary, the essential boundary conditions are imposed beforehand. The three most typical essential boundary conditions are free, simply supported (pinned), and fixed (clamped). In one dimension these boundary conditions can be mathematically expressed for the displacement  $u(x)$  as follows

$$\text{free: } \frac{\partial u}{\partial x} = \partial_x u(x) = 0, \partial_{xxx} u(x) = 0, \quad (16)$$

$$\text{simply supported: } u(x) = 0, \partial_{xx} u(x) = 0, \quad (17)$$

$$\text{fixed: } u(x) = 0, \partial_x u(x) = 0.. \quad (18)$$

When modelling the sound radiation of an instrument in the free field, the calculations are often limited over a finite volume. However, the boundary conditions at the outer surface of the volume require special attention. If they are modelled as fixed, for example, there will be artificial reflections inside the free field although they do not exist in reality. To overcome this problem, there are two solutions. Either the boundaries are modelled as so called radiating boundaries, or using a technique called Perfectly Matched Layer (PML). According to the radiating boundary condition (also called the Sommerfeld radiation condition), the sources on the surface scatter energy only to infinity, and not inside the field in question [79]. The problem is that this boundary condition works only for certain cases, for example for spherical waves. The numerically more accurate boundary condition, PML, relies on the idea that the computational domain is surrounded by an additional layer of medium that matches the computational domain and that absorbs all the incoming radiation in all angles with no reflections. The PMLs were first introduced by Berenger for electromagnetic waves. The mathematical derivation can be found in his original paper [80].

### 3.2 Formulation in the structure-acoustic domain

Both the structural and acoustic domains are governed by a set of partial differential equations [72, 73]. When deriving these equations and solving them with FEM, some assumptions are made. First of all, it is assumed that these partial differentials are linear. In the following, the domains are also considered infinite. The partial differential equations need to be formulated in a so-called weak form in order to be solved with FEM. In a weak formulation, the partial differential equation is assumed to hold for certain test functions only. In FEM, these test functions are the shape functions. Typically, the weak form equations are written in a matrix form. It is possible to represent the equations with the mechanical parameters (mass, stiffness, damping) or the modal parameters (eigenfrequencies and eigenmodes) of the system.

To begin with, in the structural domain the equation of motion for a continuous structure can be expressed with the following partial differential equation [29, 72, 73]

$$\tilde{\nabla} \boldsymbol{\sigma}_s + \mathbf{b}_s = \rho_s \ddot{\mathbf{u}}_s, \quad (19)$$

where  $\boldsymbol{\sigma}_s$  is the stress of structure,  $\mathbf{b}_s$  represents the body forces,  $\rho_s$  is the density of the material, and  $\ddot{\mathbf{u}}_s$  is the second derivate of the displacement of the structure with respect to time.  $\tilde{\nabla}$  denotes a modified gradient

$$\tilde{\nabla} = \begin{bmatrix} \partial_x & 0 & 0 & \partial_y & \partial_z & 0 \\ 0 & \partial_y & 0 & \partial_x & 0 & \partial_z \\ 0 & 0 & \partial_z & 0 & \partial_x & \partial_y \end{bmatrix}. \quad (20)$$

From this partial equation (derived, e.g., in [72, 73], the structural vibrations can be written in the weak form as follows

$$\mathbf{M}_s \ddot{\mathbf{d}}_s + \mathbf{K}_s \mathbf{d}_s = \mathbf{F}_f + \mathbf{F}_b, \quad (21)$$

where  $\mathbf{d}_s$  is the finite element approximation the displacement and  $\ddot{\mathbf{d}}_s$  its second derivate with respect to time. If damping would be introduced into the equation, it would be related to  $\dot{\mathbf{d}}_s$ .  $\mathbf{F}_f$  and  $\mathbf{F}_b$  represent the forces by the surface traction normal to the structural domain and the body of the structure, respectively.  $\mathbf{M}_s$  represents the finite element approximation of the mass of the structure over the volume  $V$  with shape functions  $\mathbf{N}$

$$\mathbf{M}_s = \int_s \mathbf{N}^T \rho_s \mathbf{N} dV. \quad (22)$$

$\mathbf{K}_s$  is the finite element approximation of the stiffness of the structure

$$\mathbf{K}_s = \int_s \tilde{\nabla} \mathbf{N}^T \mathbf{C}_s \tilde{\nabla} \mathbf{N} dV, \quad (23)$$

where  $\mathbf{C}_s$  is the stiffness matrix. The material parameters that define the stress  $\boldsymbol{\sigma}_s$  of the structure are included in the stiffness matrix. For an orthotropic material, such as wood, the stiffness matrix  $\mathbf{C}_s$  in Eq. 23 takes the following form

$$\mathbf{C}_s = \begin{bmatrix} E_x(1 - \mu_{yz}\mu_{zy})/\beta & E_x(\mu_{yz}\mu_{zx} + \mu_{yx})/\beta & E_x(\mu_{yx}\mu_{zy} + \mu_{zx})/\beta & 0 & 0 & 0 \\ E_y(\mu_{xz}\mu_{zy} + \mu_{xy})/\beta & E_y(1 - \mu_{xz}\mu_{zx})/\beta & E_y(\mu_{xy}\mu_{zx} + \mu_{zy})/\beta & 0 & 0 & 0 \\ E_z(\mu_{xy}\mu_{yz} + \mu_{xz})/\beta & E_z(\mu_{xz}\mu_{yx} + \mu_{yz})/\beta & E_z(1 - \mu_{xy}\mu_{yx})/\beta & 0 & 0 & 0 \\ 0 & 0 & 0 & G_{xy} & 0 & 0 \\ 0 & 0 & 0 & 0 & G_{xz} & 0 \\ 0 & 0 & 0 & 0 & 0 & G_{yz} \end{bmatrix}, \quad (24)$$

where  $\beta = 1 - \mu_{yz}\mu_{zy} - \mu_{xy}\mu_{yx} - \mu_{xz}\mu_{zx} - \mu_{xy}\mu_{yz}\mu_{zx} - \mu_{yx}\mu_{zy}\mu_{xz}$ ,  $\mu$  is the Poisson ratio,  $E$  the elastic moduli, and  $G$  the shear moduli.

Eq. 21 can thought of as the equation of forced harmonic vibration without damping, with mass and spring forces represented on the left-hand side, and the fluid loading and the excitation force on the right-hand side. The continuous fields over the volume have just been replaced by the shape functions over the volume.

In the acoustic domain, the partial differential equation to be considered is the equation of motion for a compressible fluid (i.e., the Helmholtz equation) [72, 73]

$$\rho_0 \ddot{\mathbf{u}}_f + \nabla p_f = 0, \quad (25)$$

where  $\rho_0$  is the density of the fluid,  $\ddot{\mathbf{u}}_f$  is the second partial derivate of displacement of the fluid with respect to time, and  $p_f$  the pressure of the fluid.  $\nabla$  denotes the gradient

$$\nabla = \begin{bmatrix} \partial_x \\ \partial_y \\ \partial_z \end{bmatrix}. \quad (26)$$

From this partial differential equation, the weak formulation in the acoustic domain becomes [72, 73]

$$\mathbf{M}_f \ddot{\mathbf{p}}_f + c_0^2 \mathbf{K}_f \mathbf{p}_f = \mathbf{F}_q + \mathbf{F}_s, \quad (27)$$

where  $\mathbf{F}_q$  and  $\mathbf{F}_s$  represent the forces by the added fluid mass and the pressure normal to the fluid domain, respectively.  $c_0$  is the speed of sound in the air.  $\mathbf{M}_f$  and  $\mathbf{K}_f$  represent again the fluid mass and its stiffness

$$\mathbf{M}_f = \int_f \mathbf{N}^T \mathbf{N} dV, \quad (28)$$

and

$$\mathbf{K}_f = \int_f \tilde{\nabla} \mathbf{N}^T \tilde{\nabla} \mathbf{N} dV. \quad (29)$$

It can be noted that the weak formulation for the structural domain (Eq. 21) and acoustic domain (Eq. 27) are in a similar form. In the coupled domain, they can be combined by defining their common boundary conditions [30, 31, 72, 73]. At the boundary of the structural and acoustic domain, the particle velocity normal to the boundary need to be continuous. With the normal vector  $\mathbf{n}$  defined pointing away from the structural boundary, this particle velocity boundary condition can written

$$\dot{\mathbf{u}}_s \cdot \mathbf{n} = \dot{\mathbf{u}}_f \cdot \mathbf{n}. \quad (30)$$

In addition, the fluid pressure causes stress on the structure in the direction of the normal. This pressure continuity boundary condition can written

$$\sigma_s \cdot \mathbf{n} = -p_f \cdot \mathbf{n}. \quad (31)$$

These two boundary conditions result into a matrix of equations [72, 73] describing the structure-acoustic domain

$$\begin{bmatrix} \mathbf{M}_s & 0 \\ \rho^0 c_0^2 \mathbf{H}_{sf}^T & \mathbf{M}_f \end{bmatrix} \begin{bmatrix} \ddot{\mathbf{d}}_s \\ \ddot{\mathbf{p}}_f \end{bmatrix} + \begin{bmatrix} \mathbf{K}_s & -\mathbf{H}_{sf} \\ 0 & c_0^2 \mathbf{K}_f \end{bmatrix} \begin{bmatrix} \mathbf{d}_s \\ \mathbf{p}_f \end{bmatrix} = \begin{bmatrix} \mathbf{F}_b \\ \mathbf{F}_q \end{bmatrix}, \quad (32)$$

where  $\mathbf{H}_{sf}$  is the spatial coupling matrix between the acoustic and the structural domain defined as the integral over the surface  $S$

$$\mathbf{H}_{sf} = \int_{\Omega_s} \mathbf{N}^T \mathbf{n} \mathbf{N} dS. \quad (33)$$

This coupling matrix stems from the boundary conditions between the structural and acoustic surface  $S$ . This interaction takes place perpendicularly to the boundary, the direction of the normal  $\mathbf{n}$ .

Changing the representation of Eq. 32 to the modal parameters, it can be formulated into [28, 72]

$$\left\{ \begin{bmatrix} \mathbf{K}_s & 0 & 0 \\ 0 & \mathbf{M}_f & 0 \\ 0 & 0 & 0 \end{bmatrix} - \omega^2 \begin{bmatrix} \mathbf{M}_s & 0 & -\mathbf{H}_{sf} \\ 0 & 0 & \mathbf{M}_f \\ \rho_0 c_0^2 \mathbf{H}_{sf}^T & \mathbf{M}_f^T & c_0^2 \mathbf{K}_f \end{bmatrix} \right\} \begin{bmatrix} \mathbf{d}_s \\ \mathbf{p}_f \\ \mathbf{q}_f \end{bmatrix} = 0, \quad (34)$$

where an additional variable  $\mathbf{q}_f$  is introduced, so that  $\mathbf{q}_f = \omega^2 \mathbf{p}_f$ .  $\omega$  is the eigenvalue of the equation. This type of matrix equations are inverted and solved for with FEM. Often, the resulting equations are more complex than Eqs. 32 and 34, as the geometries shapes are complicated.

### 3.3 Accuracy and efficiency issues

The calculation capacity and the desired accuracy set certain conditions on the meshing of the system. The accuracy of the FEM model depends on how well the shape functions approximate the behaviour of the continuous field inside the element [28, 29, 74]. In addition, the accuracy is dependent on the amount of nodal points, i.e., the amount of elements, used to approximate the continuous field and the geometry. The more complicated the geometry, the more and the smaller elements required for high accuracy. The order of the elements matters, as well. For example, if bending is modelled, at least second-order elements should be used [74]. In acoustics, a rule of thumb is to choose at least six elements per the smallest wavelength to be analysed. This stems from the fact a sine wave is considered to be acceptably represented by six line elements [30]. If there are too few elements, extra stiffness is introduced into the system. In turn, this increases the calculated eigenfrequencies of the system. Furthermore, the ratio between the largest and smallest dimension of each element should be close to unity. The more deformed in this sense the elements are, the stiffer they are, and do not necessarily represent the system stiffness realistically [74]. Many commercial softwares have automatic meshing functions that try to maximise the accuracy.

What comes to efficiency and computational load, the amount and the order of elements play an important role. Naturally, using symmetries is an efficient way to reduce the computational load of the model [29].

### 3.4 Previous work on finite element modelling of string instruments

Finite element models in acoustics are often simplified; sometimes because of unimportance of details to sound production and sometimes because of difficulties in estimating the physics. The crude approximations of the geometry and the materials were especially necessary in the early stages of FE modelling from the 1960s until the early 2000s because of limited computational capacity. In the case of string instrument modelling this meant several simplifications. For example, the strings were not considered at all, the air surrounding the instrument was omitted [42], and the material is assumed homogeneous. Most models considered instrument top plates only [27] and these were modelled using shell elements with mathematical thickness rather than normal solid elements. The frequency range was in most cases limited below 1 kHz in order to keep the number of elements and thus the degrees of freedom within a reasonable solving time [36, 42]. The amount of elements varied between a few hundred to a few thousand. For example, in the work of Bretos et al. [33] from the year 1999, the number of elements used was 9500. The enclosed air was modelled separately with specific instrument-shaped cavities [32].

Guitar soundboards have been analysed with FEM since the 1970s and violin plates since the 1980s [36]. These models have focused on the low frequency region, partially due to the importance of the lowest vibrational modes, yet mostly due to the mentioned lack of computational capacity. To illustrate these simplifications, Richardson and Roberts [42], in a paper published in 1983, modelled the top plate of the guitar in the absence of air, with fixed boundary conditions, and orthotropic material. They showed that the eigenmodes of the guitar are more sensitive to changes in plate thickness than strut thickness.

More recently, FEM has been used to study structure-acoustic coupling in musical instruments. Both enclosed and surrounding air add to the mass of the instrument and thus affect the accuracy of the FE analysis. In particular, Runnelmam et al. [35] showed that fluid loading in coupled structural-acoustic interaction has a significant impact on the eigenfrequencies of the structure and the enclosed air. The modal shapes, on the other hand, are much less affected. The model by Runnelmam et al. [35] consisted of a violin and the enclosed air. The enclosed air was modelled as one-dimensional noninteracting air column. Even though this approach neglects the three-dimensional behaviour of the air, the results agreed with the measurement fairly well below 600 Hz. Furthermore, Elejabarrieta et al. [37] modelled the coupled modes of vibration of the guitar box and the enclosed air in the low frequency region. They also obtained participation factors for top plate, back plate and air eigenmodes for each of the coupled modes. They showed that the inclusion of the air in the model significantly lowered the eigenfrequencies of the coupled guitar plates.

To understand the behavior of the enclosed fluid even better, Ezcurra et al. [39] studied the effect of the enclosed fluid on the structural modes of the guitar using three different gases. They analysed the eigenmodes of the enclosed air and the guitar body. They showed that the type of gas effects the coupling between the top and the back plate. Namely, they discovered that whenever the top and the back

plate couple, the Helmholtz resonance participates in the coupling. The shape and frequency of the Helmholtz resonance changes according to the density of the fluid. The denser the gas, the more similar were the vibration amplitudes of the top and the back plates.

The surrounding air and the radiation characteristics of string instruments have been studied with FEM less than the enclosed air. As stated previously, the surrounding air is much more efficiently modelled using BEM than FEM. Torres et al. [41] studied the radiation efficiency of higher order normal modes of the guitar top plate using FEM. They modelled the vibrational and radiation characteristics of edge and corner modes with damped harmonic analysis. They showed among other things that the guitar edge modes radiate more efficiently than the corner modes.

FEM is increasingly employed in analysing different structural changes to the instrument prior or simultaneously to building the instrument. The aim is to be able to accurately predict the behaviour of the instrument and to guide the building process into a desired direction. For example, Derveaux et al. [23] showed that the thinner the guitar plates, the more sound power they radiate. The structure-acoustic coupling was more efficient below 400 Hz for the thinner plates. Furthermore, Bretos et al. [33] showed how the carving process and the tuning of the violin plates affects the eigenmodes. They focused on the accurate description of the building blocks joining the two plates together, such as ribs and the corner blocks. In a similar manner, Elejabarrieta et al. [36] modelled the vibrational behaviour of the guitar soundboard at five different stages of construction and compared the results with measurements. They showed that the effect of structural changes on eigenmodes and eigenfrequencies is different depending on the type of boundary conditions used in the model. For example, the thickness of the soundboard affects the eigenmodes under simply supported conditions but not under free conditions. The instrument builder can often measure only the latter option while making the guitar. The most accurate results of the model when compared to measurements were obtained if the boundaries of the top plate (when attached to the ribs) were considered simply supported. Furthermore, Elejabarrieta et al. showed that the inclusion of transverse bars (braces) had a significant effect on the obtained eigenmodes and eigenfrequencies, whereas the shapes of these bars was shown not to be important. Similarly, in the modelling of piano soundboards, the inclusion of sufficient bracing has been shown to be crucial in order to reach a fair agreement with the model and the measurements [43, 47]. In addition, Torres et al. [40] compared the effect of two different bridges on the eigenmodes of the guitar top plate using FEM.

Interestingly, with a coarse estimation of the instrument geometry and boundary conditions, it is still possible to produce the main acoustical properties of the instrument. This was shown, for example, by Derveaux et al. [23] modelling the 3D sound pressure field of the guitar in the time domain with the help of spectral and fictitious domain methods. These are methods for solving partial differential equations similarly to FEM. They used a rigid back plate and simple bracing. They showed that the thinning of the guitar plates induced more changes in the presence of air than in the absence of it. This confirms the importance of including the air in the model. For further improvement between simulation and measurements, Derveaux

et al. suggested, among others, revising the damping of the fluid near boundaries with the instrument.

In addition to the necessity of modelling the air, the accuracy of FE-models can be improved by other means. In the case of wood, modelling it as orthotropic material has also been shown to be more accurate than isotropic material models [43]. Often, the material values need to be fine-tuned [36, 41]. Furthermore, the actual instruments often have the strings already attached to the body when being measured. The additional tension to the instrument soundboard caused by the strings and its effect on vibrational modes has also been studied via FEM in the case of the piano soundboard by Mamou-Mani et al.[45]. They confirmed that when strings are introduced to a flat soundboard, the eigenfrequencies of the board increase. However, when the initial crown on piano soundboard is also introduced to the model, the eigenfrequencies are initially lowered. This shows that it is important to consider which geometrical and physical features should be included in the model.

The FE-simulations have almost always been compared to measurements in order to verify the models. Ezcurra et al. [39] compared the measured and the modelled normal modes in terms of their shapes and frequency, reporting a maximum deviation of 14% at greatest. In a similar manner, Elejabarrieta et al. [36] stated that the maximum deviation between the first six measured and modelled modes is less than 1 Hz, after fine-tuning the boundary conditions. Torres et al. [40] reported 82% correspondency between the modelled and the measured normal velocity mesh. They were able to improve the similarity between the measured and modelled mobility by both making the damping frequency-dependent, and tuning the elastic properties of wood in the model. The frequency-dependent damping for the model was estimated by measuring the loss factor separately for each of the normal modes observed in the measurements.

All in all, FEM is a powerful tool for analysing structure-acoustic coupling. Simplifications are a part of the acoustic FE-models, and this often leads to some deviation between the modelled and the measured result. Based on previous research, it is essential in string instrument modelling to consider the material orthotropic, to include the most important bars and struts in the model, to treat the air as a three dimensional medium, to have the right boundary conditions, and of course, to include a sufficient number of elements in the model.

## 4 Model and measurements of a modified kantele

Modelling any geometry with FEM includes the following steps:

1. importing/drawing the geometry (with possible reductions),
2. defining material properties,
3. defining boundary conditions, and
4. meshing.

These four steps are enough to perform an eigenfrequency analysis to the geometry. For forced oscillation analysis, such as sinusoidal force analysis, one also needs to consider

5. the damping coefficient,
6. the type and location of the force, and
7. the frequency steps (sampling rate) at which the analysis is performed.

These steps for the modified kantele are described in the following. A FEM software capable of dealing with coupled domains [81] was used, since there were both structural mechanics and pressure acoustics domains. In order to solve coupled domains, the solver must be fully coupled, too [81]. A more detailed presentation of the model can be found in Appendix A. Furthermore, the FE-models are typically compared with measurements for verification. The measurement set-up used in this thesis is described in the last section of this chapter as the last step to complete the model.

### 4.1 Model geometry

First, the kantele geometry was drawn based on the physical copy, by using a computer-aided design (CAD) software [82]. The modified kantele is not symmetric in geometry, meaning that no dimension reductions due to symmetry can be made. Instead, many small geometric details were disregarded because their size was not considered to be acoustically relevant. Typically, having several small surfaces in the model leads to meshing problems in the FEM software [81]. For example, the longitudinal bars were not included in the model. Instead, the transverse bars on the plates were modelled. The bars on the back plate connect the top and the back plate together whereas the bar on the top plate stiffens the top plate. The effect of the top plate bar was studied by modelling the top plate also without it. The plastic screws and tuning pins were not modelled. A uniform thickness of 5 mm was assumed for the kantele plates, apart from the ponsi and bars inside the kantele. The real kantele back plate is slightly curved, but the modelled one was assumed to be flat. The top plate and the back plate of the model are presented in Fig. 15. Figure 16 presents the modelled kantele from the side, indicating the point of excitation, the air gap, and the sound hole. The size of air gap between the top and the back plate was varied.

The frame of the whole model including the air and the PML is presented in Fig. 17. These are both spherical domains surrounding the kantele, with the radius of  $r = 0.7$  m and  $r = 0.8$  m for the air and the PML domains, respectively.

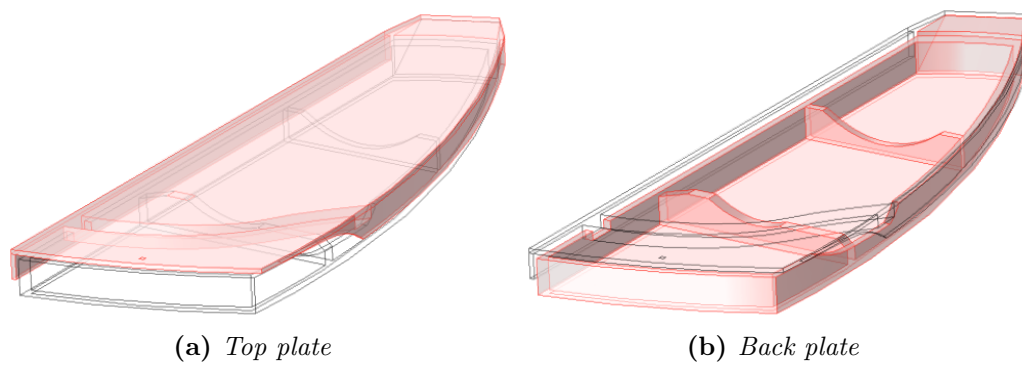


**Figure 15:** *Modelled kantele.*

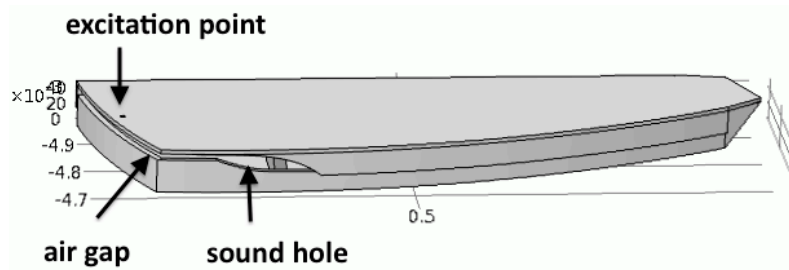


**Figure 16:** *The modelled kantele from the side with excitation point, sound hole, and the air gap included.*

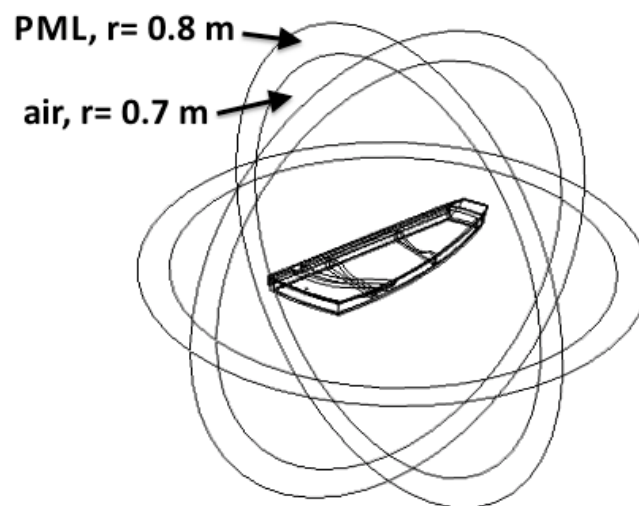


**Figure 17:** *The frame of the model with structural, air, and PML domains.*

## 4.2 Material properties

Based on previous work on instrument modelling, the material was considered orthotropic. Consequently, ten parameters for the material need to be plugged into the model: density, elastic moduli, shear moduli, and Poisson ratio in three orthogonal directions. The kantele was considered to be build from one material, spruce. In addition, the effect of changing the material to birch and pine was also investigated. The values for these wood materials were obtained from Kretschmann et al. [58]. In addition, the surrounding air domain had to be defined in terms of density and speed of sound. The PML domain was assigned with the same properties as the air domain. The material and also other parameter values used in the FE-model are presented in Tab. 2.

| Parameter             | Symbol     | Spruce | Birch | Pine | Unit                  |
|-----------------------|------------|--------|-------|------|-----------------------|
| Elastic moduli        | $E_x$      | 122    | 153   | 111  | [ $10^8$ Pa]          |
|                       | $E_y$      | 15.6   | 11.9  | 8.67 |                       |
|                       | $E_z$      | 7.20   | 7.60  | 4.22 |                       |
| Shear moduli          | $G_{xy}$   | 15.1   | 11.0  | 5.78 | [ $10^8$ Pa]          |
|                       | $G_{yz}$   | 1.22   | 2.60  | 0.56 |                       |
|                       | $G_{xz}$   | 14.6   | 10.4  | 5.33 |                       |
| Poisson ratio         | $\nu_{xy}$ | 0.42   | 0.43  | 0.33 | [1]                   |
|                       | $\nu_{yz}$ | 0.53   | 0.70  | 0.41 |                       |
|                       | $\nu_{xz}$ | 0.46   | 0.45  | 0.34 |                       |
| Density               | $\rho_s$   | 440    | 570   | 540  | [ $\text{kgm}^{-3}$ ] |
| Isotropic loss factor | $\alpha$   | 0.01   |       |      | [1]                   |
| Driving force         | $F_d$      | 1.5    |       |      | [N]                   |
| Air density           | $\rho_0$   | 1.2    |       |      | [ $\text{kgm}^{-3}$ ] |
| Speed of sound in air | $c_0$      | 343    |       |      | [ $\text{ms}^{-1}$ ]  |
| Maximum element size  | $s_{max}$  | 0.1    |       |      | [m]                   |
| Frequency resolution  | $\Delta f$ | 5      |       |      | [Hz]                  |

**Table 2:** *Parameter values inserted in the FE-model.*

## 4.3 Boundary conditions

The boundary conditions between the air and the structural domain were defined in the mathematical formulation of FEM for structure-acoustic problems (see Eqs. 30 and 31). Firstly, the particle velocity normal to the air-structure boundary is required to be continuous. Secondly, fluid loading or stress on the plates equals the air pressure normal to the air-structure boundary. The boundary condition for the surrounding air was the spherical PML domain.

## 4.4 Meshing and frequency range

Second-order tetrahedral elements with a maximum size of  $s_{max} = 0.100$  m were used in the model. With the enclosed and surrounding air included, this resulted in about 80 000 to 200 000 elements in the model depending on the size of the air gap. The degrees of freedom (DOFs) to be solved varied between 150 000 and 680 000 depending on the frequency. With this amount of DOFs, for a normal desktop computer with 8 GB of RAM and two processors it took on average 20 hours to calculate the frequency response for 15 point frequencies. This was the maximum number of DOFs that could be solved with that computer without running out of memory in the matrix factorisation. As there should be at least six elements per wavelength, the frequencies up to 570 Hz could be treated accurately with the model (with the speed of sound in air  $c_0 = 343$  ms<sup>-1</sup>). The eigenfrequency analysis was run at the frequency range of 0-570 Hz. For the sinusoidal excitation, the frequency range was limited to 70-570 Hz, with the resolution of  $\Delta f = 5$  Hz.

## 4.5 Force and damping considerations

The sinusoidal driving force  $F_d$  can be expressed as

$$F_d = Ae^{i\omega t}, \quad (35)$$

where  $A$  is the amplitude of the force,  $\omega$  is the angular frequency applied, and  $t$  is time. The frequency response was calculated to a sinusoidal force with the amplitude of  $A = 1.5$  exerted perpendicularly to the top plate. This corresponds to the approximate amplitude of plucking the kantele string with copper wire (diameter 0.05 mm) in practical experiments by the author. The copper wire plucking method enables a standard plucking procedure and is widely used [7, 62].

Following previous research [40, 56], damping is considered isotropic with the loss factor of  $\alpha = 0.01$ . The damping affects the eigenfrequencies so that [1]

$$f_{damped} = \left(1 + i\frac{\alpha}{2}\right) f_{undamped}. \quad (36)$$

Related to damping, another number describing forced vibration at a single mode or resonance is called the Q-value (or quality factor) [1], defined as

$$Q = \frac{\pi f}{\alpha}. \quad (37)$$

Q-value indicates how sharp the peak of the resonance is, and how wide its excitation band in frequency is. The higher the Q-value, the sharper the resonance.

## 4.6 Measurements

In order to verify the model, measurements with the kantele were carried out in an anechoic chamber where the anechoic conditions apply above 60 Hz. The modified kantele with a 5-mm air gap was excited with an impulse hammer (PCB Piezotronics Impulse Force Hammer 086C01). The response was recorded using an external sound card (MOTU Traveller Lite mk3) at a sample rate of 44.1 kHz with a microphone (Rode NT1-A) at 1 m above the middle of the kantele top plate. The excitation point was the same as in the model, i.e., in the middle of the top plate, 5 mm away from the free edge (see Fig. 16). The strings were damped, and the kantele was held on the ponsi, so that it was hanging in the air. The set-up is shown in Fig. 18. Afterwards, the microphone response was compensated with the input force from the hammer according to Eq. 6. The impulse hammer was not calibrated.



**Figure 18:** *Measurement set-up*

## 5 Results

The results of this thesis can be divided into four parts. Firstly, as a side-product of improving the correspondence between the measured and the modelled kantele, several structural changes on the kantele have been modelled. They illustrate how FEM can be used in string instrument design. Secondly, the modified kantele is compared to the traditional kanteles in terms of vibrational modes and radiation. Thirdly, the effect of the air gap size on the modified kantele is studied. Finally, the radiation efficiency of the different kanteles is compared. Before introducing the results, the FE-simulation is compared with the measurements and the differences between these two are accounted for.

### 5.1 Experimental and modelled frequency responses

It is an iterative process to arrive at the best possible agreement between the measurement and the simulation. Oftentimes, there is a limit to the similarity that depends on the computational capacity and the awareness of the complexity of the underlying physical phenomena. In the case of musical instruments this could be related, for example, to the complexity of the damping of both wood and air or to the boundary conditions.

The measured and modelled frequency responses at 0.7 metres above the kantele are shown in Fig. 19. The measured frequency response has been scaled down so that visual comparison is reasonable. The material in the FE-model of the kantele is spruce and the air gap is 5 mm.

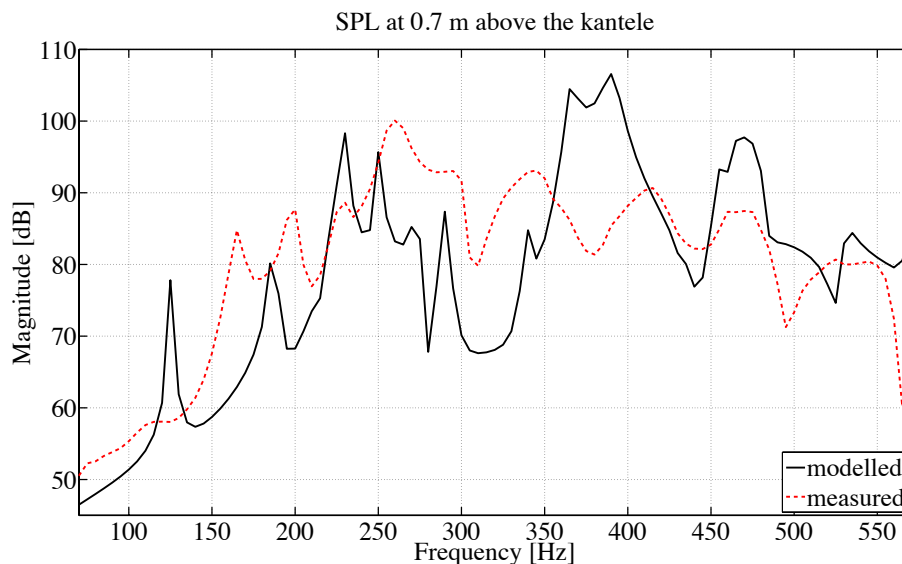


**Figure 19:** *The frequency responses at 0.7 m above the kantele for the modelled kantele (solid black line) and the measured kantele (dashed red line). The material is spruce and the air gap between the top and the back plate is 5 mm.*

By visual inspection, it can be seen that the overall shape of the two responses is similar. Some frequencies of the normal modes as well as the overall sound pressure

level differ. Furthermore, in some cases the modelled normal modes are much sharper than the measured ones. In other words, the modelled Q-values are higher than the measured Q-values. This shows that the Q-values, and thus the loss factor, are frequency-dependent in reality. The overall difference in the measured and modelled sound pressure levels is caused by many factors, such as microphone sensitivity, voltage settings, and difference in the excitation magnitude. The model is excited sinusoidally with amplitude  $A = 1.5$  N while the measurements were done with an impulse hammer with a higher excitation magnitude.

The relative similarity between the two frequency responses was calculated to be 76% using the definition by Deecke et al. [83]. This is comparable to reported correspondences in previous research. For example, Torres et al. [40] reported a similarity of 82%. In most cases, the compared variables have been the measured and the modelled eigenmodes and eigenfrequencies rather than frequency responses. Following that example, the greatest difference between the modelled and the measured modes is 40 Hz. This occurs between the first modelled and the first measured mode. This yields a maximum deviation of 24% between the measured and the modelled frequencies. In previous work, Ezcurra et al. [39], for example, reported a maximum mode frequency difference of 14%.

When comparing the similarity values of the current model to previous research, an important distinction must be made. In previous research, the focus of modelling has been either on the top plate only or the top and the back plate connected with ribs only. The modified kantele in this thesis has a more complicated connection between the plates. Namely, the plates are connected with three thin plastic screws at three points on the top plate. The way such connections should be modelled is not straightforward. For this reason, the FE-model of the top plate is also compared with the measured modified kantele. This comparison is shown in Fig. 20.

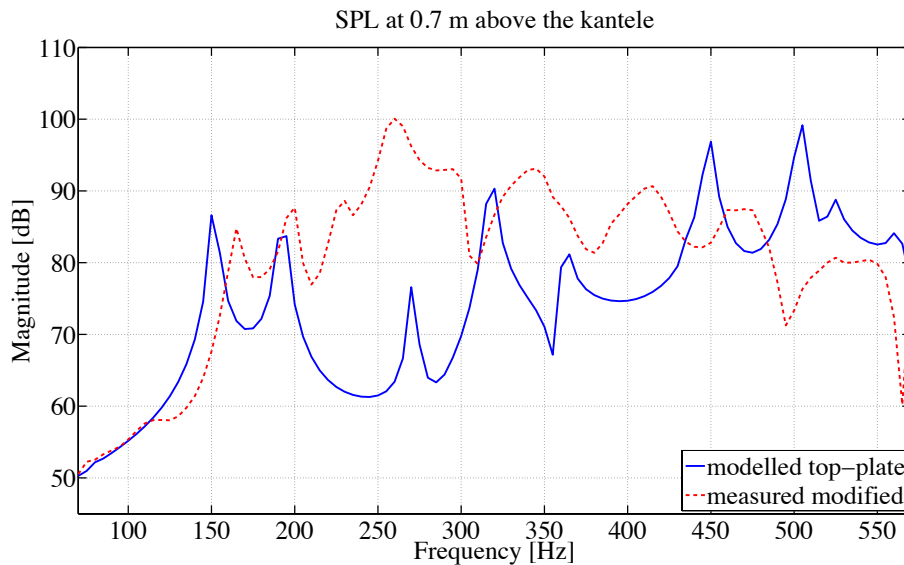


**Figure 20:** The frequency responses at 0.7 m above the kantele for the modelled top-plate kantele (solid blue line), and the measured modified kantele (dashed red line).

As can be seen, the first two normal modes of the simulated top plate are close to the first two measured normal modes. The mode shapes of the simulated top plate are the same as those of the simulated modified kantele, but their frequencies are higher for the top plate. What is more, the back plate is not involved in these mode shapes. In conclusion, in the FE-model, the top plate couples more strongly to the back plate than in reality. However, the simulated top plate corresponds better to the measured kantele in regard to the first two normal modes.

Consequently, the model of the modified kantele could be improved by revising the connection between the top and back plate. In reality, the two are connected with three plastic screws. In the model, the connection is established through three wooden blocks. The screws are small elements and modelling them accurately would increase the amount of elements in the model significantly. The present model was already at the limits of the available computation capacity. Therefore, a whole new approach for the model should be taken, e.g., by using shells elements, in order to improve the correspondence between the FE-model and the built kantele.

Other factors also contribute to the differences between the measured and the modelled frequency responses. The measured kantele includes the strings and the tuning pins, which add stiffness to the top plate. The transverse load of the strings has been found to increase the eigenfrequencies when the magnitude of the load is comparable to the thickness of the plate [46]. Additional stiffness and mode damping is also caused by thin longitudinal bars on the real kantele top plate. Furthermore, the back plate was modelled flat, even though in reality, it is slightly curved. In addition, the material parameters for wood in the model were estimated from literature [58]. In reality, the material properties of wood vary significantly depending on, e.g., the moisture content and growing location. In addition, the damping coefficients vary considerably for wood used in sound boards [56]. In previous research, fine-tuning of the parameters has been an issue [36, 41].

## 5.2 Structural and material changes

FEM provides an interesting tool for studying structural and material changes of musical instruments without building them. In addition, it is essential to study what kind of assumptions and simplifications about the structure can be made in the model without compromising the correspondence to the measured values. For these purposes, the following three cases of a structural change are presented for the modified kantele:

1. including and excluding the transversal bar on the top plate,
2. kantele made of different wooden materials, and
3. top plate and back plate made of different materials.

In the first case, the frequency responses of the kantele with and without the bar under the tuning pins on the top plate are shown in Fig. 21. The solid black line represents the kantele with the bar and the dashed red line represents the kantele without the bar. It can be seen that in an instrument like the kantele, a transverse bar has an effect on the frequency response.

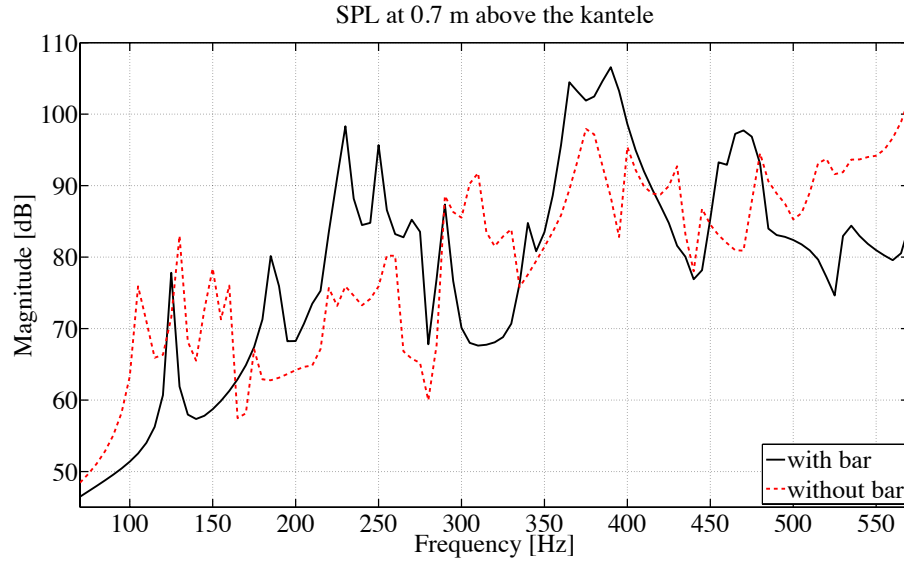


**Figure 21:** *The frequency responses at 0.7 m above the kantele with the bar (solid black line), and without the bar (dashed red line).*

Mainly, it makes the free edge of the kantele top plate stiffer. To give an example, the five mode peaks that appear below 200 Hz in the barless kantele collapse to two in the kantele with the bar. More precisely, when the shapes of normal modes are studied, it can be noticed that the modes (2,0) at 105 Hz and (2,0)-(0,2) at 150 Hz shift in frequency, to 125 Hz and 185 Hz, respectively, while the mode shapes remain unaffected. The other three normal modes at 130 Hz, 160 Hz, and 175 Hz, whose mode shapes relate to the free edge vibrating, disappear when the bar is introduced. This confirms the importance of including the transverse bars of the top plate in modelling stated in previous research [36].

In the second case, the kantele is made of different materials. The frequency responses are shown in Fig. 22 for spruce (solid black line), pine (dashed red line) and birch (dash-dotted blue line) according to the values in Tab. 2. By visual inspection, the overall shape of the frequency responses for different materials is similar except that it shifts in frequency. For example, the first normal mode shifts from 125 Hz to 120 Hz and to 80 Hz for spruce, birch and pine, respectively. In a similar manner, the third normal mode shifts 230 Hz - 220 Hz - 165 Hz. The mode shapes remain unaffected. Of these materials, birch has the highest density, which explains the lowered mode frequencies compared to spruce. Pine is density-wise between spruce and birch but it is much softer than the two. This is why in the case of pine the modes are even lower in frequency than those in the case of spruce and birch.

The third case is when the top and the back plate are made of different materials. In the example, the top plate is made of spruce and the back plate of birch. The frequency responses at 0.7 m above the kantele are represented by the solid black line for the uniform kantele, and the dashed red line for the kantele with two materials. Birch is a much denser material than spruce and thus the modes react to the

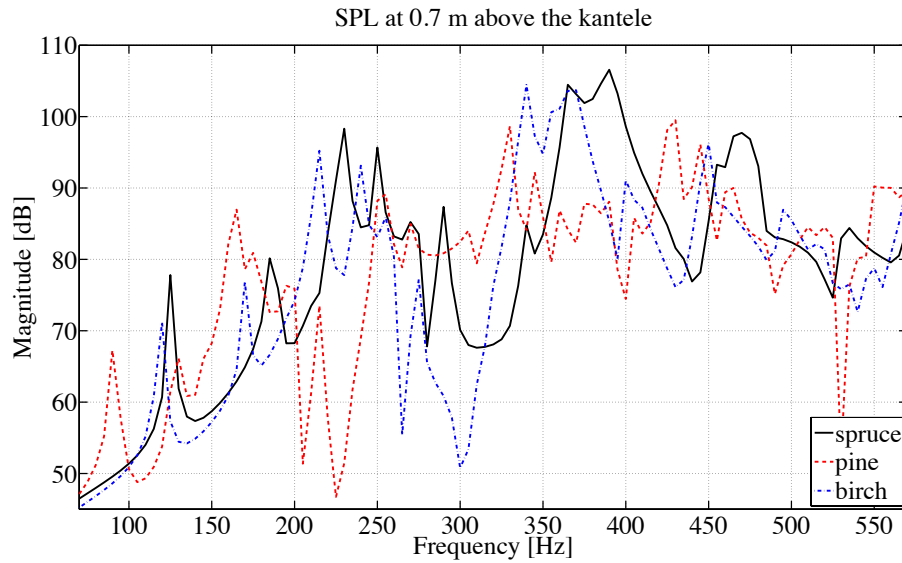


**Figure 22:** The frequency responses at 0.7 m above the kantele made of spruce (solid black line), pine (dashed red line), and birch (dash-dotted line).

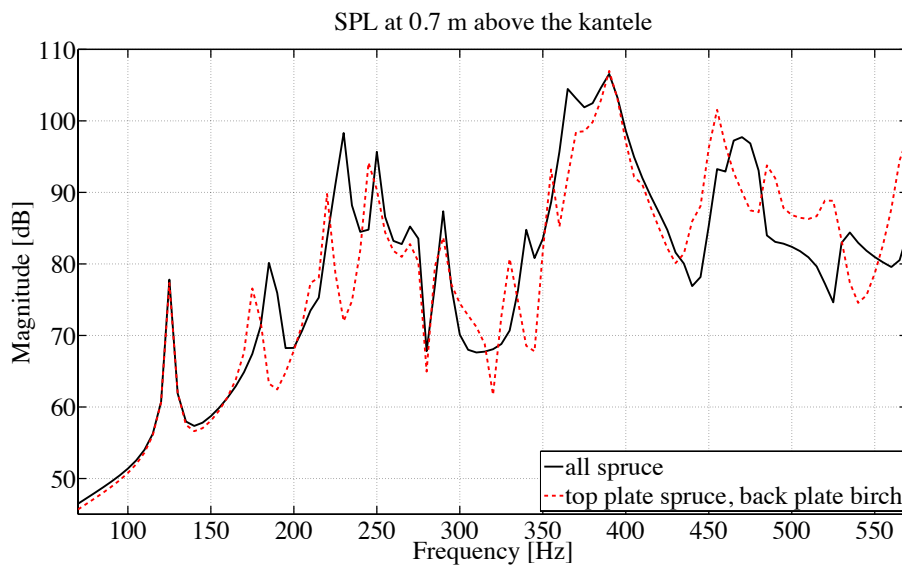


**Figure 23:** The frequency responses at 0.7 m above the kantele made of one material, spruce, (solid black line), and two materials: top plate made of spruce and back plate made of birch (dashed red line).

increased mass by shifting lower in frequency. This is why the densities have been reduced to  $\rho_{\text{spruce}} = 400 \text{ kgm}^{-3}$  and  $\rho_{\text{birch}} = 520 \text{ kgm}^{-3}$ . It can be seen, the overall shape of the frequency responses is similar. The changes in mode frequencies are subtle. For example, the frequency difference of the first two normal modes becomes smaller.

### 5.3 Comparison of traditional and modified kanteles

In addition to the modified kantele, there are the two traditional kantele structures: the box kantele and the top-plate kantele. These three structures can be compared by regarding the modified kantele with no air gap as the box kantele (with a sound hole on the side), and the top plate of the modified kantele as the top-plate kantele. The frequency responses at 0.7 m above the kantele for these three different structures are presented in Fig. 24. The box kantele is presented by the dash-dotted red line, the modified kantele by the solid black line and the top-plate kantele by the dashed blue line. Based on the figure, the structures differ at least in overall sound pressure level, mode density, and mode frequencies. The box kantele has a lower sound pressure level than the top-plate and the modified kantele, except at 295 Hz and at 555 Hz. The modal density between 70-570 Hz is 7, 9 and 11 for the box, top-plate, and modified kantele, respectively. The modelled frequency range covers almost entirely the tuning range of strings, 73-588 Hz. It is desirable to have many modes in this range for better sound quality and level [15]. This is one of the factors that explain the increased loudness of the modified kantele compared to the traditional top-plate kantele observed by Penttinen et al. [18].

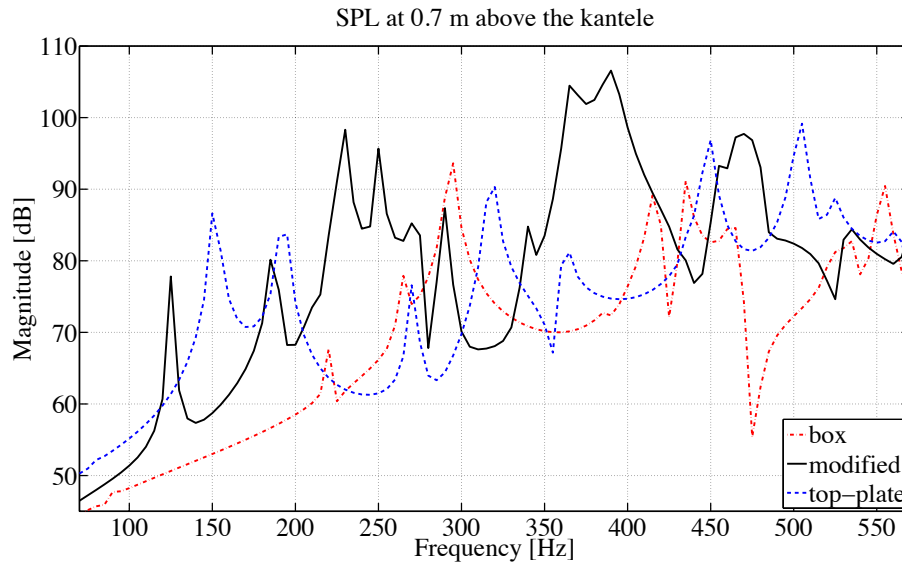


**Figure 24:** The sound pressure level at 0.7 m above the kantele for three different kantele structures: box kantele (dash-dotted red line), modified kantele (solid black line) and top-plate kantele (dashed blue line).

The mode density for the modified kantele is higher than for the two traditional kanteles because the modified kantele includes modes of both the top-plate kantele and the box kantele. In other words, the modified kantele has a freely vibrating top plate and the air enclosed by the two plates which can couple to the plate vibrations. An example of this case is illustrated in Fig. 25. Figure 25a) shows the first two normal mode shapes of the top-plate kantele (at 150 Hz and 195 Hz), Fig. 25b) the first significant normal mode of the box kantele (at 295 Hz), and Fig. 25c) the first three normal modes of the modified kantele (at 125 Hz, 185 Hz, and 230 Hz). The

color legend indicates the total displacement in millimeters. The values above and below the legend are the maximum and minimum values for the displacement. It can be seen that shapes of the first two top plate modes correspond to the shapes of the first two normal modes of the modified kantele. The frequencies of these modes have changed, from 150 Hz to 125 Hz, and from 195 Hz to 185 Hz. In addition, the vibration amplitudes (total displacement) are smaller for the modified kantele than for the top-plate kantele. In particular, the ponsi vibrates less. The back plate has a solid ponsi, which is fixed to the top plate, and thus adds mass to that part of the kantele.

Similarly, the shape of first significant normal mode of the box kantele corresponds to the shape of the third normal mode of the modified kantele. The mode frequency has changed from 295 Hz to 230 Hz. The only difference between these two shapes is that in the modified kantele, the free edge also has a vibration maximum. In addition, the Helmholtz resonance and the back plate participate in the vibration. For this mode, the vibration amplitude is higher for the modified kantele than for the box kantele.

Figure 26 shows the corresponding sound pressure levels for the mode shapes in Fig. 25; the first two normal modes of the top-plate kantele are shown in Fig. 26a), the first significant normal mode of the box kantele in Fig. 26b), and the first three normal modes of the modified kantele in Fig. 26c). The color legend indicates the sound pressure level in decibels. The values above and below the legend are the maximum and minimum values for the sound pressure level, respectively. It can be seen that the radiation of the modified kantele at these three modes is more omnidirectional than for the traditional kanteles. The top-plate kantele has a higher maximum sound pressure level, but it also has some directions on the sides where sound radiation is small. This is a demonstration of the acoustic short-circuit.

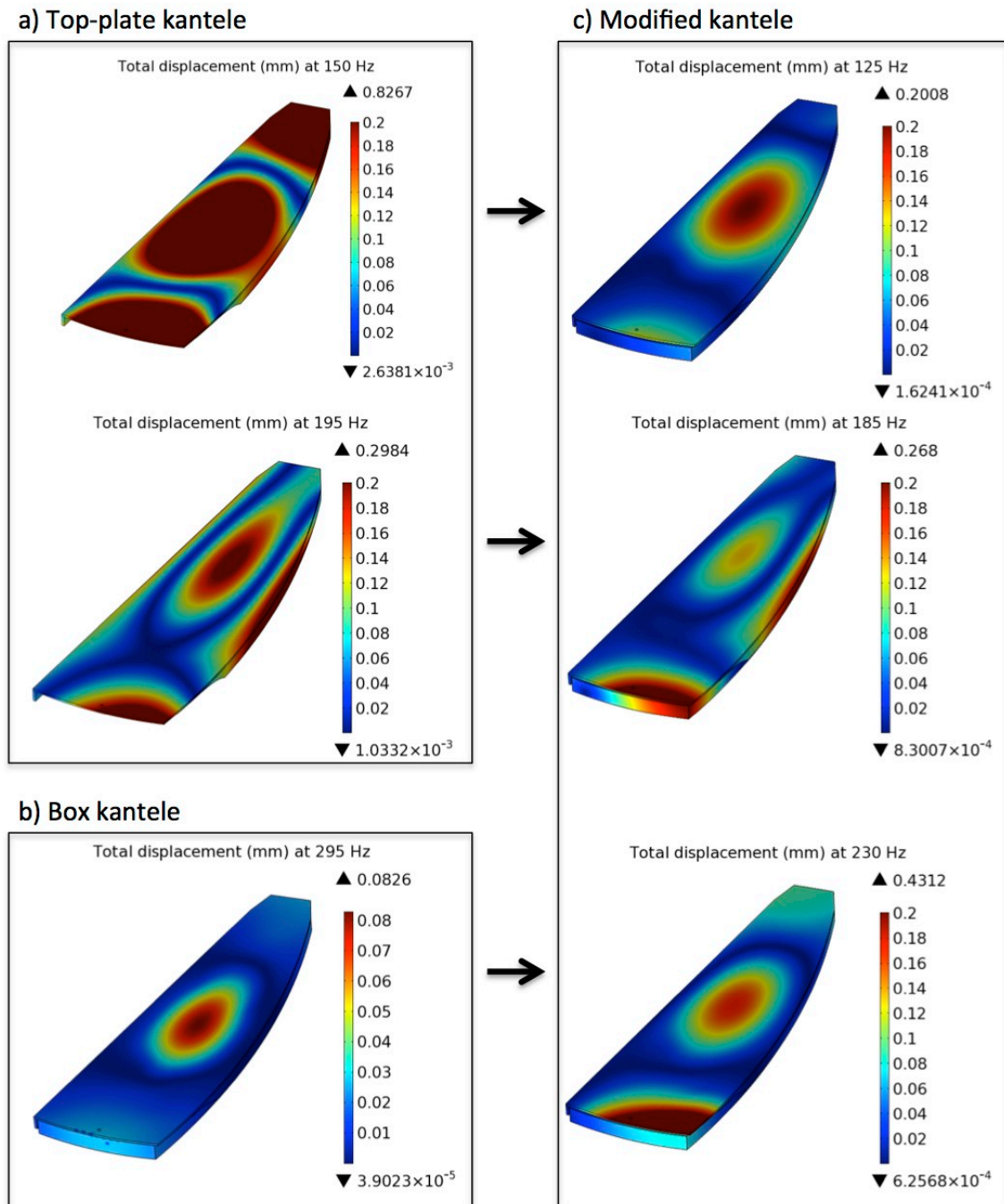


**Figure 25:** An example of how the modified kantele includes normal modes of both the top-plate kantele and the box kantele in terms of total displacement. In a) the first two normal modes of the top-plate kantele, in b) the first normal mode of the box kantele, and c) the first three normal modes of the modified kantele. The mode shapes that are on the same row correspond to one another.

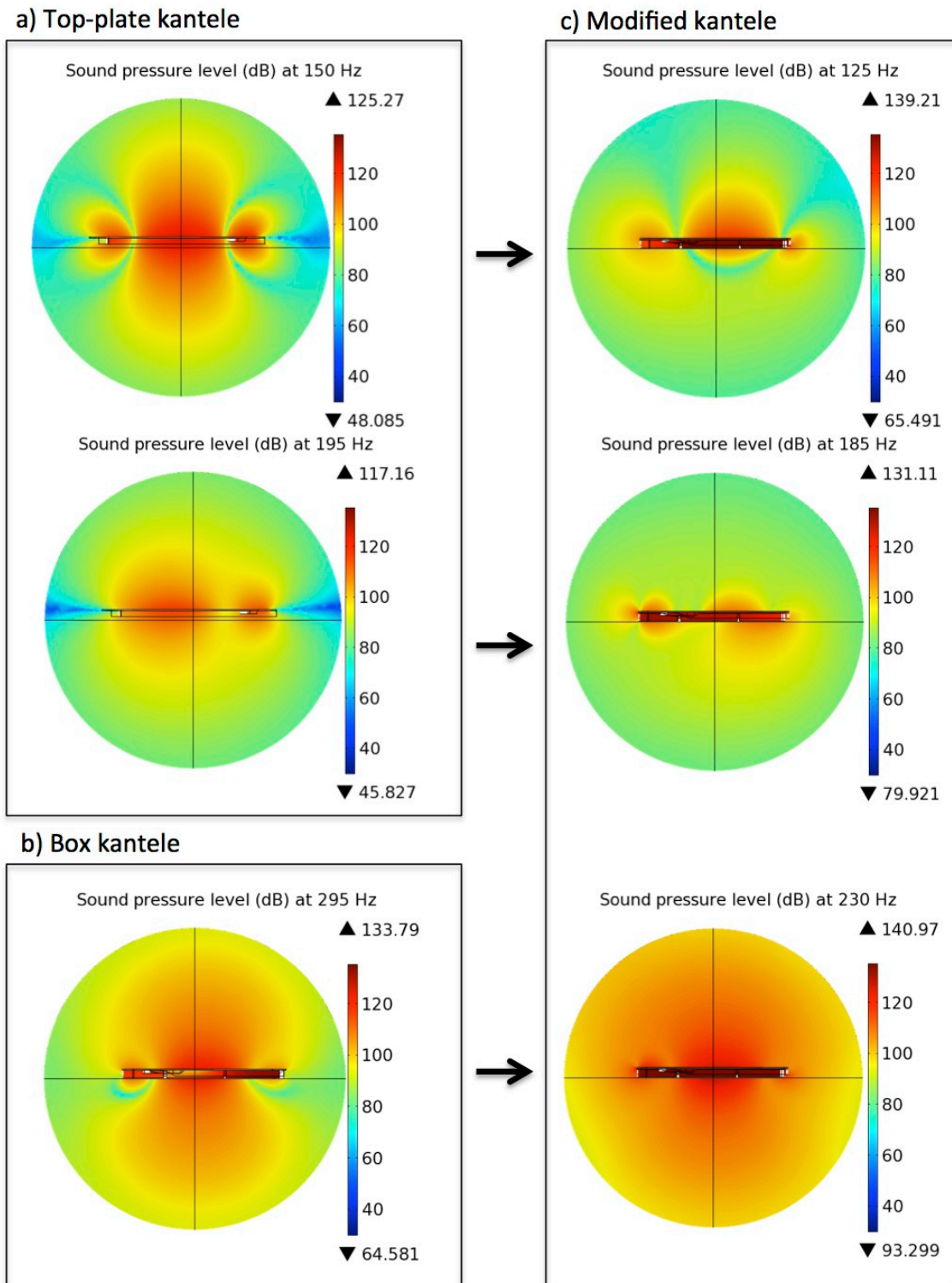


**Figure 26:** An example of how the modified kantele includes normal modes of both the top-plate kantele and the box kantele in terms of sound pressure levels. In a) the first two normal modes of the top-plate kantele, in b) the first normal mode of the box kantele, and c) the first three normal modes of the modified kantele. The mode shapes that are on the same row correspond to one another. The kantele soundhole is facing the reader.

## 5.4 Effects of different air gap sizes

The size of the air gap in the modified kantele can be changed. It is of interest to study how the size effects the vibrational and radiation properties of the kantele. Indeed, already a small air gap between the top and back plate changes the frequency response. Figure 27 shows the modelled frequency responses for the kantele with different air gaps: 1 mm, 3 mm, and 7 mm.

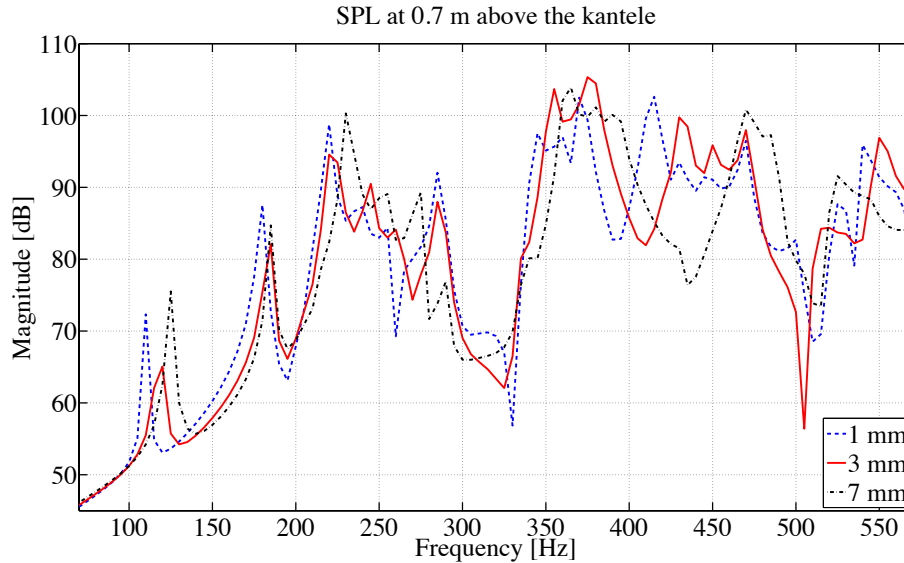


**Figure 27:** The frequency responses at 0.7 metres above the kantele with different air gaps: 1 mm (dashed blue line), 3 mm (solid red line), and 7 mm (dash-dotted black line).

Based on Fig. 27, two different frequency ranges for the changes can be distinguished. First of all, below 300 Hz the mode density does not change, but the mode frequencies increase when the size of the air gap increases. The mode shapes do not change, but their vibration amplitudes do. Secondly, above 300 Hz, the mode density decreases when the size of the air gaps increases. In addition, the modes shapes do not appear in the same order in frequency. This means that some normal modes appear higher in frequency and some lower in frequency. For example, for the 5-mm air gap, the combination of the top plate mode shape (1,2) and the back plate mode shape (2,0) occurs at 470 Hz. For the 3-mm air gap, this mode shape is at 450 Hz, even though it also has a normal mode at 470 Hz. Because the frequency responses change with the size of the air gap, this size variation could be considered a timbral controller, at least, for the instrument builder, and possibly for the player.

As the size of the air gap increases, the free edge of the top plate is able to vibrate more freely. What is more, the vibration maxima move closer to the edges and the back plate is less coupled with the top plate. An example of a mode that undergoes such a change is the sixth normal mode of the modified kantele, occurring at 285 Hz. It experiences a drop of 15 dB in sound pressure level when the size of the air gaps increases for 1 mm to 7 mm. In addition, its frequency shifts to 290 Hz.

This mode shape is shown in Fig. 28 for different sizes of air gaps: 3 mm, 5 mm, and 7 mm. The case with the 1-mm air gap is almost identical to the 3-mm air gap. In the left column the kantele is seen from above and in the right column from the bottom. The corresponding sound pressure level and pressure fields are shown in Fig. 29. With the increasing air gap size, several phenomena occur. Firstly, it can be observed that the coupling of the top and the back plate decreases. The back plate vibrates with the shape (2,0) and its vibration amplitude decreases with the increase of the air gap. Furthermore, the widths of the vibration maxima decrease. At the free edge, the vibration maximum moves towards the corner that is the least fixed. In addition, the radiation patterns become more directive since the width of vibration maxima decrease. Finally, different air modes couple with the body: for 3-mm and 5-mm air gaps, the air vibrates with the mode shape (2,0), and for the 7-mm air gap with (1,0).

## 5.5 Radiation efficiency

The modified kantele has a higher mode density than the traditional kanteles. It also seems that the vibration maxima and sound pressure level decrease when the size of the air gap increases, at least for some modes. But this does not describe the overall picture. For the entire frequency range, the average radiation efficiency describes how effective the different structures actually are in transmitting input energy to radiation. The averaged radiation efficiencies for the kantele with different air gaps are shown in Tab. 3. It also includes the radiation efficiencies of the traditional kantele bodies. Comparing the box kantele to the modified kantele with 1-mm air gap, it can be seen that the radiation efficiency increases by 50% when the air gap is added between the plates. The radiation efficiency is at its maximum with the 3-mm air gap. Beyond that, the radiation efficiency becomes comparable to that of the box kantele. Thus, there is an optimum size of the air gap in terms of radiation efficiency. The top-plate kantele has the lowest radiation efficiency of all the structures studied. It also exhibits more directional radiation patterns.

| Air gap  | box    | 1 mm   | 3 mm          | 5 mm   | 7 mm   | top-plate |
|----------|--------|--------|---------------|--------|--------|-----------|
| $\sigma$ | 0.0159 | 0.0242 | <b>0.0281</b> | 0.0128 | 0.0083 | 0.0008    |

**Table 3:** Radiation efficiency of the kantele with different air gaps, and the traditional box and top-plate kanteles.

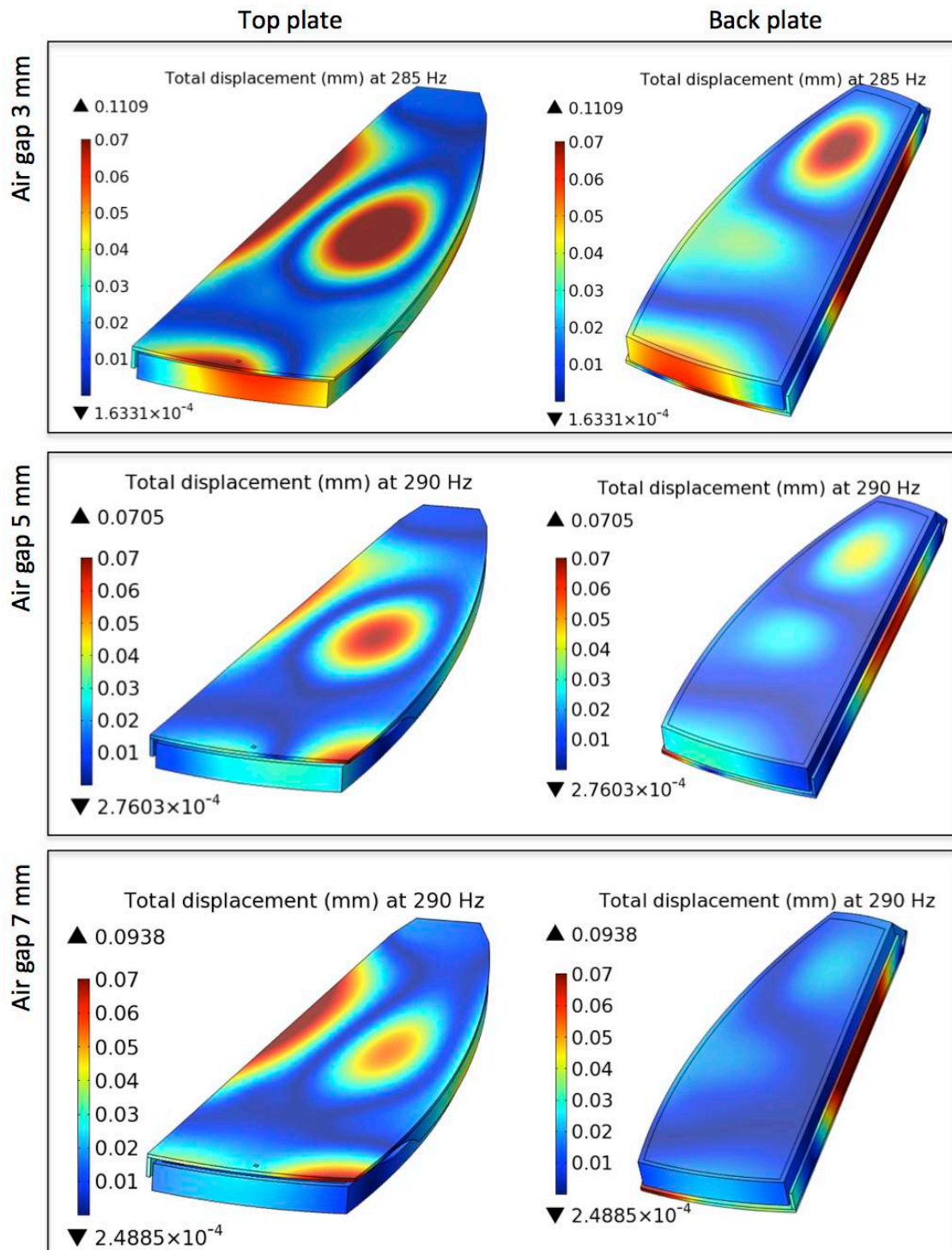


**Figure 28:** *Vibration amplitudes of the sixth normal mode of the modified kantele with an air gap of 3 mm, 5 mm, and 7 mm. In the left-hand column the kantele is seen from the top and in the right-hand column from the bottom.*

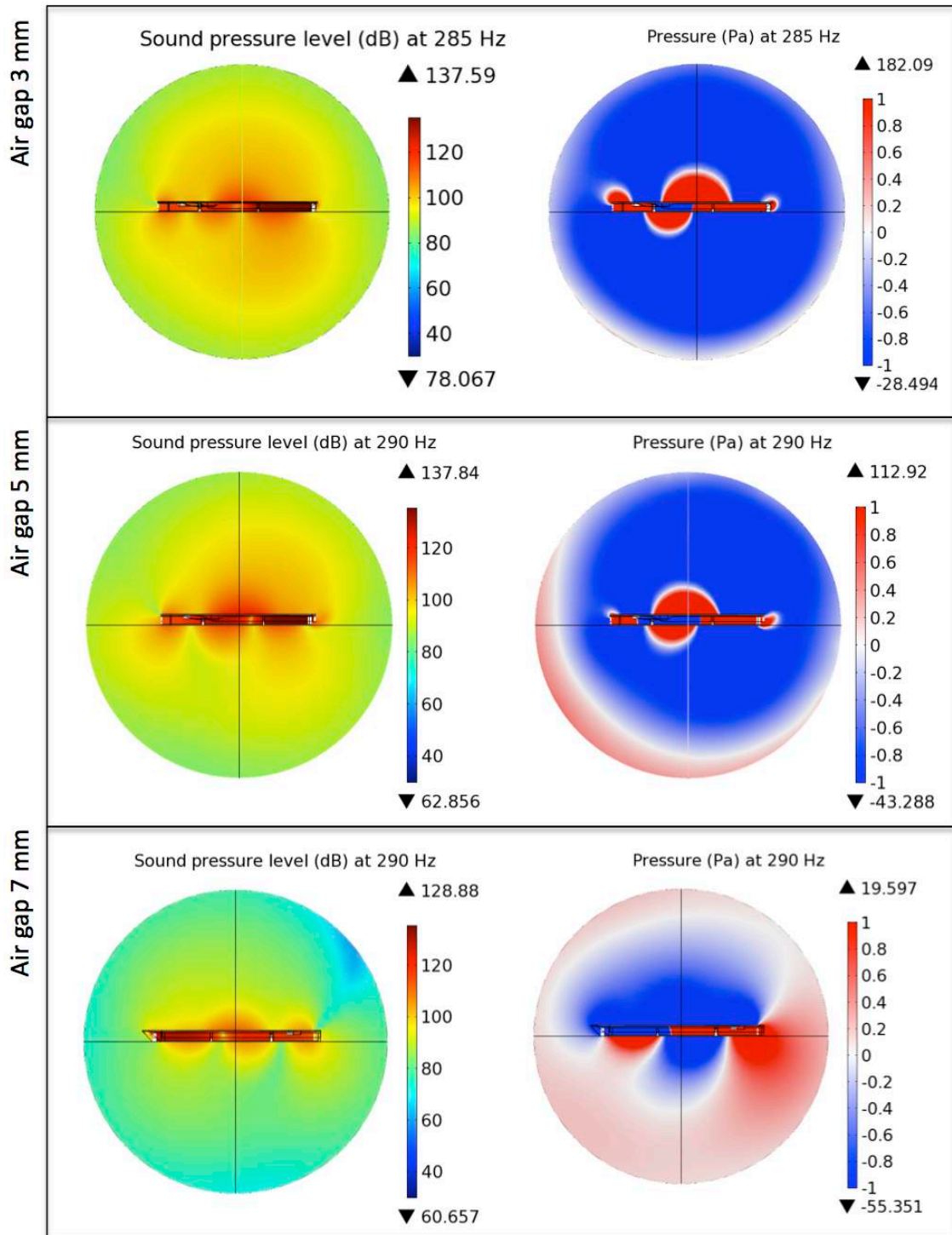


**Figure 29:** The sound pressure level and pressure of the sixth normal modes on the modified kantele with an air gap of 3 mm, 5 mm, and 7 mm. The sound pressure level is on the left-hand column and the pressure on the right-hand column.

## 5.6 Eigenfrequencies and Helmholtz resonance

More insight to the coupling between the air and the kantele body is gained through the eigenfrequency analysis. Figure 30 shows the eigenfrequencies below 570 Hz of the kantele body and the enclosed air, both separately and when coupled. The bar on the top plate under the tuning pins is not included in the model due to meshing problems. The air gap between the top plate and the back plate is a) 0 mm, b) 5 mm, and c) 10 mm. Several observations based on the eigenfrequencies can be made. First of all, the coupled eigenfrequencies are lower than those of the enclosed air and the body separately, in all three cases. It has been verified previously that enclosed air acts as added mass to the body and thus the coupled eigenfrequencies are lower [35, 39]. Secondly, there are more eigenmodes (both coupled and individual parts) in the presence of the air gap than in the absence of it.

The eigenfrequencies of the enclosed air, represented by the red dots in Fig. 30, are also affected by the air gap. When the air gap is introduced, the first air eigenfrequency decreases and the second increases. This would suggest that the first air eigenfrequency is inversely related to the air volume, meaning that it is the Helmholtz resonance. Thus, the Helmholtz resonance would then be at 227 Hz for the modified kantele with 5 mm air gap. The second eigenfrequency could relate to the mass of the air.

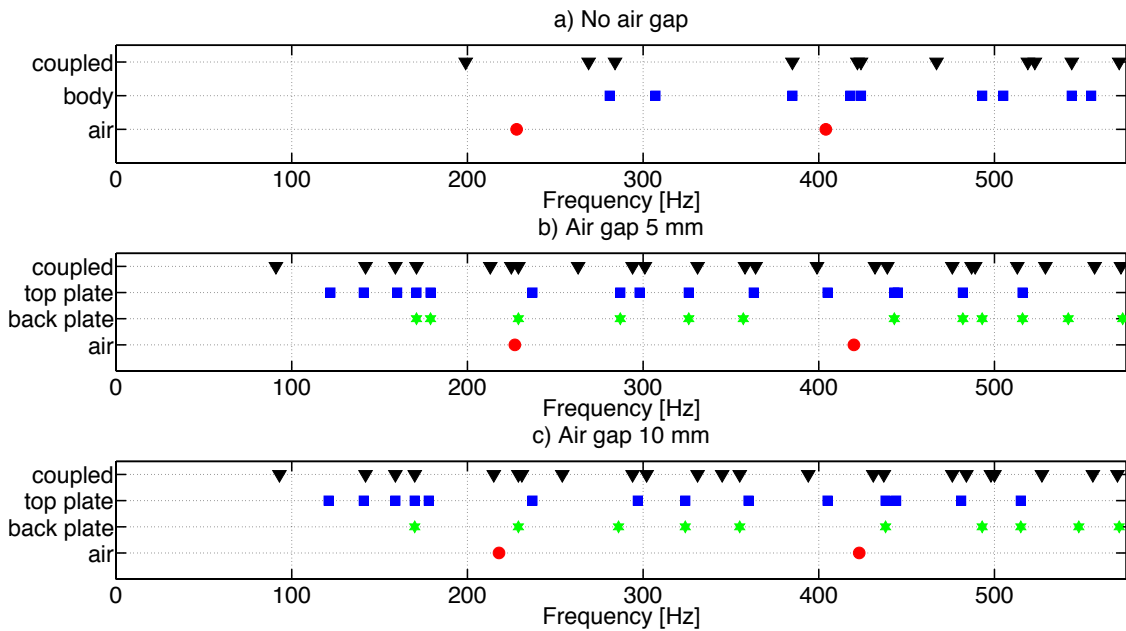


**Figure 30:** The eigenfrequencies below 570 Hz when the size of the air gap is a) 0 mm, b) 5 mm, and c) 10 mm. The geometry does not include the bar on the top plate.

## 6 Conclusions and future work

In this thesis, the body of a string instrument called the kantele has been modelled with the finite element method. Both the eigenfrequency analysis and forced vibration analysis with sinusoidal excitation were used to simulate the kantele with the frequency range of 70-570 Hz. Three models of the body were included; two traditional structures, the top-plate kantele and the box kantele, were compared with a modified kantele which has an air gap separating the top and the back plate. In the modified kantele, the top plate acts as a free-edge vibrator. In particular, the tuning pin edge of the kantele is able to vibrate freely, because the side has been removed. In addition, together the top and the back plate create an enclosed air mass that has its own vibrational modes.

Combining both the freely vibrating top plate and the enclosed air leads to an increased density of normal modes and eigenmodes in the modified kantele in comparison to the traditional kanteles. The radiation efficiency of the modified kantele is also improved compared to the traditional kanteles, provided that the air gap is small. Of the sizes modelled, an air gap of 3 mm had the highest radiation efficiency.

The enclosed air also allows air modes, in particular the Helmholtz resonance, to couple with the plate modes. Thus, the radiation patterns of the modified kantele are more omni-directional than those of the traditional kanteles. This phenomenon also contributes to the increased radiation efficiency of the modified kantele. The Helmholtz resonance of the modified kantele occurs at around 230 Hz. The specific value depends on the size of the air gap which affects the air volume.

The analyzed frequency range covers almost entirely the tuning range of the strings, i.e., 73-588 Hz. The higher mode density in this range is beneficial for the sound quality and level of the instrument, as the string vibrations couple better with the body. This is one of the reasons for the improved loudness of the modified kantele compared to the traditional kanteles.

There are three main directions for future work. Firstly, the FE-model could be made to correspond closer to the built kantele. Several parts of the kantele were not modelled due to computational complexity. The FE-model focused on the body only. Yet, the instrument also includes tuning pins and strings that play an important role in the vibrational behaviour of the whole instrument. One concrete suggestion would be to model the acoustic behaviour of the body under string excitation in order to obtain a better picture of the instrument when played. This could be done, for example, by adding tuning pins to the model that are excited by a force measured at a real tuning pin during string excitation. Then, the pre-stress caused by the strings on the body would have to be modelled mathematically. Including the strings themselves in the model might be an option if the amount of elements in the body model can first be decreased. This requires a new starting point for the model, and possibly combining different modelling methods, such as the boundary element method, with the finite element method. In order to improve the correspondence between the model and the measurement, perhaps an alternative approach could be to make a simpler physical copy of the kantele to be measured.

Secondly, the freely vibrating top plate structure could be applied to other instruments, such as mandolin, piano, and guitar. In particular, it could be useful for instruments in need of increased loudness and timbral variation, especially at lower frequencies. In addition, a mechanism that allows the air gap size to be varied by the kantele player might offer an interesting tool for additional expression and timbre modification.

Finally, the current FE-model serves as a basis for sound synthesis. The frequency responses obtained with the model could be convolved with a string model. In addition, the obtained radiation patterns could be used for room simulations with the kantele as a sound source.

## References

- [1] N. H. Fletcher and T. D. Rossing, *The Physics of Musical Instruments*. Springer Verlag, 2nd ed., 1998.
- [2] A. Moral and E. Jansson, “Input admittance, eigenmodes, and quality of violins,” tech. rep., KTH Royal Institute of Technology, Department of Speech, Music, and Hearing, Stockholm, Sweden, 1982.
- [3] J. Meyer, “Quality aspects of the guitar tone,” in *Function, Construction, and Quality of the Guitar*, Stockholm, Sweden: KTH Royal Institute of Technology, Department of Speech, Music, and Hearing, 1983.
- [4] J. Woodhouse, “The acoustics of A0-B0 mode matching in the violin,” *Acta Acustica*, vol. 84, pp. 947–956, 1998.
- [5] V. Välimäki, J. Pakarinen, C. Erkut, and M. Karjalainen, “Discrete-time modelling of musical instruments,” *Report on Progress in Physics*, vol. 69, no. 1, pp. 1–78, 2006.
- [6] M. Tinnsten and P. Carlsson, “Numerical optimization of violin top plates,” *Acta Acustica united with Acustica*, vol. 88, pp. 278–285, 2002.
- [7] J. Woodhouse, “Body vibration of the violin – what can a maker expect to control?,” *Journal of the Catgut Acoustical Society*, vol. 4, no. 5, pp. 43–49, 2002.
- [8] C. Hutchins, “Founding a family of fiddles,” *Physics Today*, vol. 20, pp. 23–37, 1967.
- [9] P. Jalkanen, H. Laitinen, and A.-L. Tenhunen, *Kantele*. Finnish Literature Society SKS, 2010.
- [10] A. Smolander-Hauvonen, *Paul Salminen – Suomalaisen konserttikanteleen ja soittotekniikan kehittäminen*. PhD thesis, Sibelius Academy, Helsinki, Finland, 1998.
- [11] M. Karjalainen, J. Backman, and J. Pölkki, “Analysis, modeling, and real-time sound synthesis of the kantele, a traditional Finnish string instrument,” in *Proceedings of IEEE International Conference on Acoustics, Speech, and Signal Processing*, (Minneapolis, Minnesota, USA), pp. 229–232, 1993.
- [12] C. Erkut, M. Karjalainen, P. Huang, and V. Välimäki, “Acoustical analysis and model-based sound synthesis of the kantele,” *Journal of the Acoustical Society of America*, vol. 112, no. 4, pp. 1681–1691, 2002.
- [13] J. Pakarinen, M. Karjalainen, and V. Välimäki, “Modeling and real-time synthesis of the kantele using distributed tension modulation,” in *Proceedings of the Stockholm Music Acoustics Conference*, (Sweden), 2003.

- [14] V. Välimäki, M. Karjalainen, T. Tolonen, and C. Erkut, “Nonlinear modeling and Synthesis of the kantele – a traditional Finnish string instrument,” in *Proceedings of International Computer Music Conference*, (Beijing, China), 1999.
- [15] A. Peekna and T. D. Rossing, “Acoustics of carved baltic psalteries,” *Acta Acustica united with Acustica*, vol. 91, pp. 269–276, 2005.
- [16] J. Pölkki, C. Erkut, H. Penttinen, M. Karjalainen, and V. Välimäki, “New designs for the kantele with improved sound radiation,” in *Proceedings of the Stockholm Music Acoustic Conference*, (Sweden), 2003.
- [17] H. Penttinen, C. Erkut, J. Pölkki, V. Välimäki, and M. Karjalainen, “Design and analysis of a modified kantele with increased loudness,” *Acta Acustica united with Acustica*, vol. 91, pp. 261–268, 2005.
- [18] H. Penttinen, *Loudness and Timbre Issues in Plucked Stringed Instruments – Analysis, Synthesis, and Design*. PhD thesis, Helsinki University of Technology, Espoo, Finland, 2006.
- [19] S. Bilbao, *Numerical Sound Synthesis: Finite Difference Schemes and Simulation in Musical Acoustics*. John Wiley and Sons, 2009.
- [20] L. Hiller and P. Ruiz, “Synthesizing musical sound by solve the wave equation for vibrating objects: Parts I and II,” *Journal of the Audio Engineering Society*, vol. 19, no. 6/7, 1971.
- [21] P. A. A. Esquef, M. Karjalainen, and V. Välimäki, “Frequency-zooming ARMA modeling for analysis of noisy string instrument tones,” *EURASIP Journal on Applied Signal Processing*, vol. 10, pp. 953–967, 2003.
- [22] C. Vyasarayani, S. Birkett, and J. McPhee, “Modeling the dynamics of a vibrating string with a finite distributed unilateral constraint: application to the sitar,” *Journal of the Acoustical Society of America*, vol. 125, no. 6, pp. 3673–3682, 2009.
- [23] G. Derveaux, A. Chaigne, P. Joly, and E. Becache, “Time-domain simulation of a guitar: Model and method,” *Journal of the Acoustical Society of America*, vol. 114, no. 6, pp. 3368–3383, 2003.
- [24] H. Penttinen, M. Karjalainen, T. Paatero, and H. Järveläinen, “New techniques to model reverberant instrument body responses,” in *Proceedings of International Computer Music Conference*, (La Habana, Cuba), 2001.
- [25] M. Karjalainen and J. Smith, “Body modeling techniques for string instrument synthesis,” in *Proceedings of International Computer Music Conference*, (Hong Kong), 1996.

- [26] B. Richardson, “Numerical modelling of stringed musical instruments,” in *Proceedings of the Stockholm Music Acoustics Conference*, (Sweden), 1993.
- [27] A. Chaigne, “Modeling and simulation of musical instruments,” in *Proceedings of Forum Acusticum*, (Aalborg, Denmark), 2011.
- [28] O. Zienkiewicz and R. Taylor, *The Finite Element Method: Volume I, The Basis*. Butterworth-Heinemann, 5th ed., 2000.
- [29] N. Ottosen and H. Pettersson, *Introduction to Finite Element Method*. Prentice Hall International, 1992.
- [30] F. Ihlenburg, *Finite Element Analysis of Acoustic Scattering*. Springer, 1998.
- [31] A. Graggs, “Acoustic modeling: Finite element method,” in *Handbook of Acoustics* (M. Crocker, ed.), pp. 149–157, John Wiley and Sons Inc., 1998.
- [32] J. Bretos, C. Santamaria, and J. A. Moral, “Vibrational patterns of a violin-shaped air cavity obtained by finite element modeling,” *Acta Acustica united with Acustica*, vol. 85, pp. 584–586, 1999.
- [33] J. Bretos, C. Santamaria, and J. A. Moral, “Vibrational patterns and frequency responses of the free plates and box of a violin obtained by finite element analysis,” *Journal of the Acoustical Society of America*, vol. 105, no. 3, pp. 1942–1950, 1999.
- [34] C. Buksnowitz, A. Teishinger, U. Möller, A. Pahler, and R. Evans, “Resonance wood [*Picea abies* L.]—evaluation and prediction of violin makers’ quality rating,” *Journal of the Acoustical Society of America*, vol. 121, no. 4, pp. 2384–2395, 2007.
- [35] A. Runnemalm, *Sound and Vibrations in Structures with Air Closures*. PhD thesis, Luleå University of Technology, Sweden, 1999.
- [36] M. J. Elejabarrieta, A. Ezcurra, and C. Santamaría, “Vibrational behaviour of the guitar soundboard analysed by the finite element method,” *Acta Acustica united with Acustica*, vol. 87, pp. 128–136, 2001.
- [37] M. J. Elejabarrieta, A. Ezcurra, and C. Santamaría, “Evolution of the vibrational behavior of a guitar soundboard along successive construction phases by means of modal analysis technique,” *Journal of the Acoustical Society of America*, vol. 108, no. 1, pp. 369–378, 2000.
- [38] M. J. Elejabarrieta, A. Ezcurra, and C. Santamaría, “Coupled modes of the resonance box of the guitar,” *Journal of the Acoustical Society of America*, vol. 111, no. 5, pp. 2283–2292, 2002.
- [39] A. Ezcurra, M. Elejabarrieta, and C. Santamaria, “Fluid-structure coupling in the guitar box: numerical and experimental comparative study,” *Applied Acoustics*, vol. 66, pp. 411–425, 2005.

- [40] J. A. Torres and R. Boullosa, “Influence of the bridge on the vibrations of the top plate of a classical guitar,” *Applied Acoustics*, vol. 70, pp. 1371–1377, 2009.
- [41] J. A. Torres and R. Boullosa, “Radiation efficiency of a guitar top plate linked with edge or corner modes and intercell cancellation,” *Journal of the Acoustical Society of America*, vol. 130, no. 1, pp. 546–556, 2011.
- [42] B. Richarson and G. Roberts, “The adjustment of mode frequencies in guitars: a study by means of holographic interferometry and finite element analysis,” in *Proceedings of the Stockholm Music Acoustics Conference*, (Sweden), 1983.
- [43] N. Giordano, “Simple model of a piano soundboard,” *Journal of the Acoustical Society of America*, vol. 102, no. 2, pp. 1159–1168, 1996.
- [44] J. Berthaut, M. Ichchou, and L. Jezequel, “Piano soundboard: structural behaviour, numerical and experimental study in the modal range,” *Applied Acoustics*, vol. 63, pp. 1113–1136, 2003.
- [45] A. Mamou-Mani, J. Frelat, and C. Besnainou, “Numerical simulation of a piano soundboard under downbearing,” *Journal of the Acoustical Society of America*, vol. 123, no. 4, pp. 2401–2406, 2008.
- [46] A. Mamou-Mani, J. Frelat, and C. Besnainou, “Prestressed soundboards: Analytical approach using simple systems including geometrical nonlinearity,” *Acta Acustica united with Acustica*, vol. 95, pp. 915–928, 2009.
- [47] L. Ortiz-Berenguer, F. Casajus-Quiros, E. Blanco-Martin, and D. Ibanez-Cuenca, “Modeling of piano sounds using FEM simulation of soundboard vibration,” in *Proceedings Forum Acusticum*, (Paris, France), 2008.
- [48] H. Laitinen and H. Saha, *A Guide to Five String Kantele Playing*. Kaustinen, Finland: Folk Music Institute, 1988.
- [49] T. D. Rossing, R. F. Moore, and P. A. Wheeler, *Science of Sound*. Addison Wesley, 3rd ed., 2001.
- [50] C. Valette, “The mechanics of vibrating strings,” in *Mechanics of Musical Instruments* (A. Hirschberg, J. Kergomard, and G. Weinreich, eds.), pp. 115–184, Springer, 1995.
- [51] B. Bank and H.-M. Lehtonen, “Perception of longitudinal components in piano string vibrations,” *Journal of the Acoustical Society of America Express Letters*, vol. 128, no. 3, 2010.
- [52] K. A. Legge and N. H. Fletcher, “Nonlinear generation of missing modes on a vibrating string,” *Journal of the Acoustical Society of America*, vol. 76, no. 1, pp. 5–12, 1984.
- [53] J. Rae, “Banjo,” in *The Science of String Instruments* (T. D. Rossing, ed.), pp. 59–75, Springer, 2010.

- [54] D. Peterson, “Hammered dulcimer,” in *The Science of String Instruments* (T. D. Rossing, ed.), pp. 371–392, Springer, 2010.
- [55] S. Yoshikawa, “Acoustical classification of woods for string instruments,” *Journal of the Acoustical Society of America*, vol. 122, no. 1, pp. 568–573, 2007.
- [56] U. Weigst, “Wood for sound,” *American Journal of Botany*, vol. 93, no. 10, pp. 1439–1448, 2006.
- [57] V. Bucur, *Acoustics of Wood*. CRC Press, 1995.
- [58] D. Kretschmann, “Chapter 5. mechanical properties of wood,” in *Wood Handbook*, no. FPL-GTR-190 in Technical Report, U.S. Department of Agriculture, Forest Service, Forest Laboratory, 2010.
- [59] L. Cremer, M. Heckl, and E. Ungar, *Structure-Borne Sound*. Springer Verlag, 2nd ed., 1988.
- [60] F. Fahy, *Sound and Structural Vibration*. Academic Press, 4th ed., 1994.
- [61] E. Magliula and J. McDaniel, “Flexural wave dispersion in orthotropic plates with heavy fluid loading,” *Journal of the Acoustical Society of America Express Letters*, vol. 123, no. 5, 2008.
- [62] K. D. Marshall, “Modal analysis of a violin,” *Journal of the Acoustical Society of America*, vol. 77, no. 2, pp. 695–709, 1985.
- [63] G. Weinreich, “Coupled piano strings,” *Journal of the Acoustical Society of America*, vol. 62, no. 6, pp. 1474–1484, 1977.
- [64] Cremer, *Physics of the Violin*. Research Studies Press, 2nd ed., 2000.
- [65] J.-L. L. Carrou, F. Gautier, N. Dauchez, and J. Gilbert, “Modelling of sympathetic string vibrations,” *Acta Acustica united with Acustica*, vol. 91, pp. 277–288, 2004.
- [66] O. Christensen and B. Vistisen, “Simple model for low-frequency guitar function,” *Journal of the Acoustical Society of America*, vol. 68, no. 3, pp. 758–766, 1980.
- [67] T. Lahti, “Akustinen mittaustekniikka,” tech. rep., Laboratory of Acoustics and Audio Signal Processing, Helsinki University of Technology, Espoo, Finland, 1995.
- [68] F. Zotter, *Analysis and Synthesis of Sound Radiation with Spherical Arrays*. PhD thesis, University of Music and Performing Arts Graz, Austria, 2009.
- [69] G. Bissinger, “Structural acoustics of good and bad violins,” *Journal of the Acoustical Society of America*, vol. 124, no. 3, pp. 1764–1773, 2008.

- [70] H. Suzuki, “Vibration and sound radiation of a piano soundboard,” *Journal of the Acoustical Society of America*, vol. 80, no. 6, pp. 1573–1582, 1986.
- [71] J. Pätynen, V. Pulkki, and T. Lokki, “Anechoic recording system for symphony orchestra,” *Acta Acustica united with Acustica*, vol. 94, pp. 856–865, 2008.
- [72] G. Everstine, “Finite element formulations of structural acoustics problems,” *Computers and Structures*, vol. 65, no. 3, pp. 307–321, 1997.
- [73] P. Davidsson, *Structure-Acoustic Analysis; Finite Element Modelling and Reduction Methods*. PhD thesis, Lund University, Sweden, 2004.
- [74] P. Kurowski, *Finite Element Analysis for Design Engineers*. SAE International, 2004.
- [75] A. Seybert and T. Wu, “Acoustic modeling: Boundary element methods,” in *Handbook of Acoustics* (M. Crocker, ed.), pp. 158–168, John Wiley and Sons Inc., 1998.
- [76] B. Finlayson, *The Method of Weighted Residuals and Variational Principle*. Academic Press, 1972.
- [77] A. Chaigne and A. Askenfelt, “Numerical simulations of piano string. I. A physical model for a struck string using finite difference methods,” *Journal of the Acoustical Society of America*, vol. 90, no. 2, pp. 1112–1118, 1994.
- [78] R. Bader, “Fine tuning of the guitar sounds with changed top plate, back plate and rim geometry using a whole body 3D Finite-Difference model,” in *Proceedings Forum Acusticum*, (Paris, France), 2008.
- [79] O. Zienkiewicz, D. Kelly, and P. Bettess, “The Sommerfeld (radiation) condition on infinite domains and its modelling in numerical procedures,” in *Computing Methods in Applied Sciences and Engineering*, vol. I, pp. 169–203, Springer, 1977.
- [80] J.-P. Berenger, “A perfectly matched layer for the absorption of electromagnetic waves,” *Computational Physics*, vol. 114, pp. 185–200, 1994.
- [81] COMSOL Multiphysics, version 4.2.0.228. <http://www.comsol.com>, October 2012.
- [82] Rhinoceros, version OS X Wenatchee (work-in-progress). <http://www.rhino3d.com>, October 2012.
- [83] V. Deecke and V. Janik, “Automated categorization of bioacoustic signals: Avoiding perceptual pitfalls,” *Journal of the Acoustical Society of America*, vol. 119, no. 1, pp. 645–653, 2006.

# A Appendix

An example of a COMSOL model of the modified kantele.

## Contents

1. [Model 1 \(mod1\)](#)
  - 1.1. [Definitions](#)
  - 1.2. [Geometry 1](#)
  - 1.3. [Materials](#)
  - 1.4. [Acoustic-Solid Interaction \(acsl\)](#)
  - 1.5. [Mesh 1](#)

## 1. Model 1 (mod1)

### 1.1. Definitions

#### 1.1.1. Variables

Variables 1

Selection

|                        |              |
|------------------------|--------------|
| Geometric entity level | Entire model |
|------------------------|--------------|

| Name    | Expression  | Description |
|---------|---|-------------|
| rho_air | 1.2[kg/m^3]   |             |
| c_air   | 343[m/s]  |             |
| P_r     | $(4 \cdot \pi \cdot r_s^2 / N) \cdot \text{intop1}(\text{abs}(p^2) / (\text{rho\_air} \cdot c\_air))$ |             |
| N       | intop1(1)   |             |
| r_s     | 0.7[m]  |             |
| v_d     | $\text{sqrt}(\text{acsl.uAmp\_tX}^2 + \text{acsl.uAmp\_tY}^2 + \text{acsl.uAmp\_tZ}^2)$               |             |
| v_avg   | intop2(v_d^2)/N2  |             |
| N2      | intop2(1)   |             |
| P_i     | real(F_d*conj(v_d))   |             |
| F_d     | 1.5[N]  |             |
| P_eff   | P_r/P_i   |             |
| rad_eff | $P_r / (\text{rho\_air} \cdot c\_air \cdot v\_avg \cdot S)$   |             |
| S       | intop3(1)   |             |

#### 1.1.2. Model couplings

Integration 1

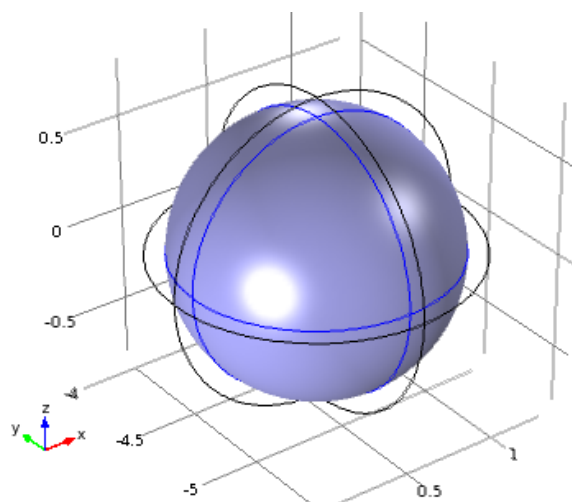
|               |             |
|---------------|-------------|
| Coupling type | Integration |
| Operator name | intop1      |

Source selection

|                        |                              |
|------------------------|------------------------------|
| Geometric entity level | Boundary                     |
| Selection              | Boundaries 5-8, 49-50, 52-53 |

Settings

| Name   | Value     |
|--------|-----------|
| Method | summation |



*Source selection*

### Integration 2

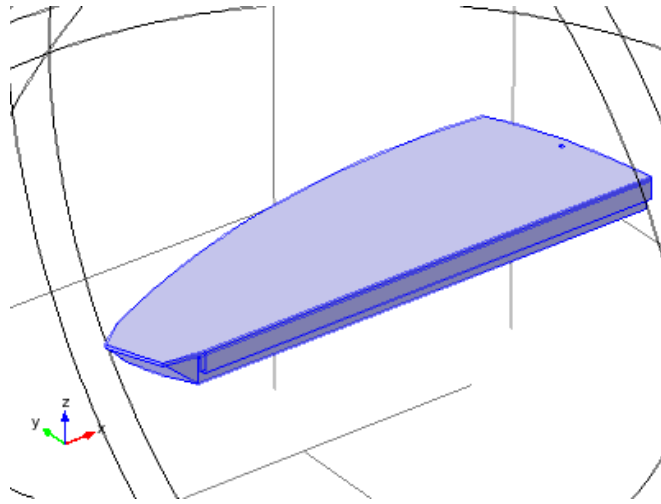
|               |             |
|---------------|-------------|
| Coupling type | Integration |
| Operator name | intop2      |

Source selection

|                        |  |
|------------------------|--|
| Geometric entity level | Boundary   |
| Selection              | Boundaries 9-10, 12, 14-15, 17-22, 24-25, 28, 32, 34-37, 59, 83-84 |

Settings

| Name   | Value     |
|--------|-----------|
| Method | summation |



*Source selection*

### Integration 3

|               |             |
|---------------|-------------|
| Coupling type | Integration |
| Operator name | intop3      |

Source selection

|                        |  |
|------------------------|--|
| Geometric entity level | Boundary   |
| Selection              | Boundaries 9-10, 12, 14-15, 17-22, 24-25, 28, 32, 34-37, 59, 83-84 |

## 1.2. Geometry 1

Geometry statistics

| Property             | Value |
|----------------------|-------|
| Space dimension      | 3     |
| Number of domains    | 4     |
| Number of boundaries | 86    |
| Number of edges      | 212   |
| Number of vertices   | 133   |

### 1.2.1. Import 1 (imp1)

Settings

| Name            | Value   |
|-----------------|---|
| Geometry import | cad   |
| Filename        | /Users/htahvana/Documents/FINAL COMSOL MODELS/distances/kantele_bar_7.sat |

|          |     |
|----------|-----|
| Surfaces | off |
|----------|-----|

### 1.2.2. Work Plane 1 (wp1)

#### Settings

| Name       | Value        |
|------------|--------------|
| Plane type | faceparallel |

### 1.2.3. Sphere 1 (sph1)

#### Settings

| Name     | Value          |
|----------|----------------|
| Position | {0.5, -4.8, 0} |
| x        | 0.5            |
| y        | -4.8           |
| Axis     | {0, 0, 1}      |
| Axis     | {0, 0, 1}      |
| Radius   | 0.7            |

### 1.2.4. Sphere 2 (sph2)

#### Settings

| Name     | Value          |
|----------|----------------|
| Position | {0.5, -4.8, 0} |
| x        | 0.5            |
| y        | -4.8           |
| Axis     | {0, 0, 1}      |
| Axis     | {0, 0, 1}      |
| Radius   | 0.8            |

## 1.3. Materials

### 1.3.1. Spruce 440

#### Selection

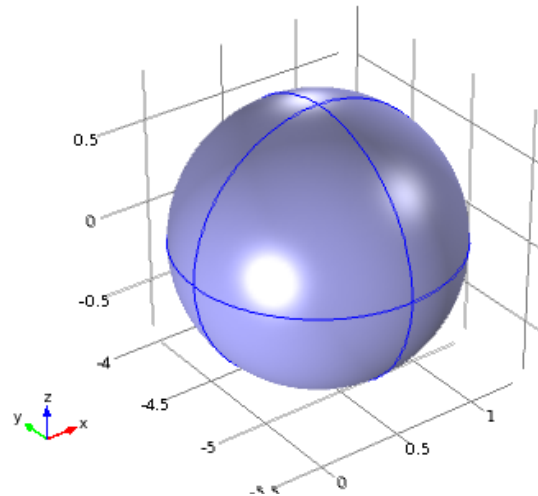
|                        |             |
|------------------------|-------------|
| Geometric entity level | Domain      |
| Selection              | Domains 1-4 |

#### Material parameters

| Name            | Value                  | Unit              |
|-----------------|------------------------|-------------------|
| Density         | 440                    | kg/m <sup>3</sup> |
| Young's modulus | {122e8, 15.6e8, 7.2e8} | Pa                |

|   |                          |    |
|---|--------------------------|----|
| Poisson's ratio                             | {0.42, 0.53, 0.46}       | 1  |
| Shear modulus                               | {15.1e8, 1.22e8, 14.6e8} | Pa |
| Loss factor for orthotropic Young's modulus | {0.01, 0.01, 0.01}       | 1  |
| Loss factor for orthotropic shear modulus   | {0.01, 0.01, 0.01}       | 1  |

#### 1.4. Acoustic-Solid Interaction (acsl)



*Acoustic-Solid Interaction*

Selection

|                        |             |
|------------------------|-------------|
| Geometric entity level | Domain      |
| Selection              | Domains 1-4 |

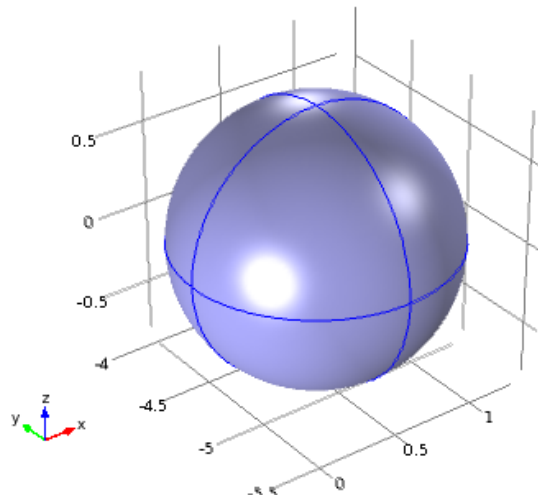
##### 1.4.1. Pressure Acoustics Model 1

Settings

Settings

| Description    | Value        |
|----------------|--------------|
| Density        | User defined |
| Density        | 1.2          |
| Speed of sound | User defined |
| Speed of sound | 343          |

##### 1.4.2. Sound Hard Boundary (Wall) 1

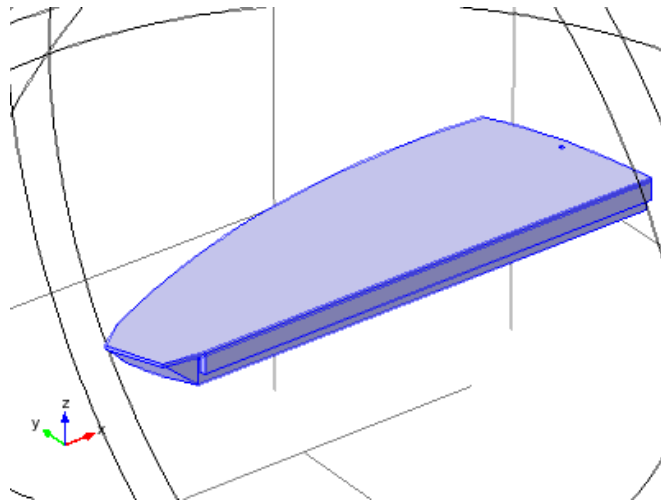


*Sound Hard Boundary (Wall) 1*

Selection

|                        |                               |
|------------------------|-------------------------------|
| Geometric entity level | Boundary                      |
| Selection              | Boundaries 1-4, 47-48, 51, 54 |

#### 1.4.3. Acoustic-Structure Boundary 1

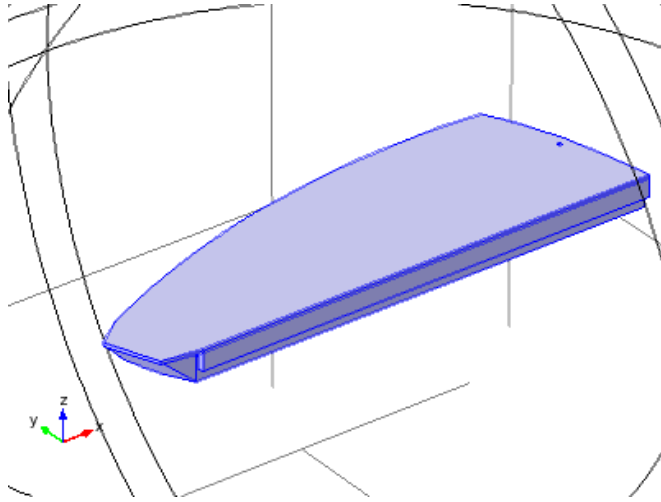


*Acoustic-Structure Boundary 1*

Selection

|                        |  |
|------------------------|--|
| Geometric entity level | Boundary   |
| Selection              | Boundaries 9-15, 17-46, 55-63, 65, 70-71, 73-77, 80, 82-86 |

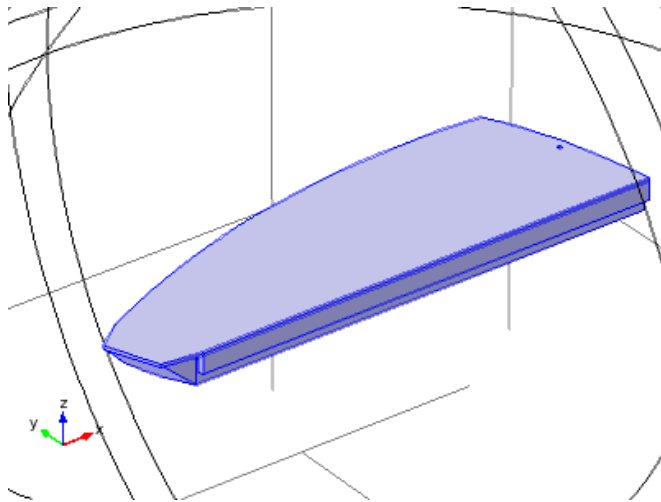
#### 1.4.4. Linear Elastic Material Model 1



*Linear Elastic Material Model 1*

| Selection              |             |
|------------------------|-------------|
| Geometric entity level | Domain      |
| Selection              | Domains 3-4 |

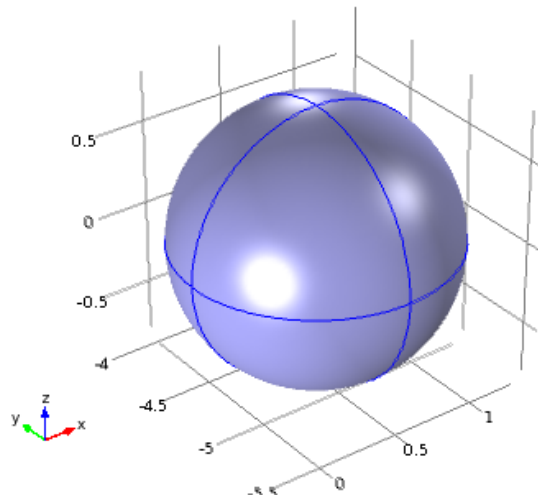
**Damping 1**



*Damping 1*

| Selection              |             |
|------------------------|-------------|
| Geometric entity level | Domain      |
| Selection              | Domains 3-4 |

**1.4.5. Perfectly Matched Layers 1**



*Perfectly Matched Layers 1*

Selection

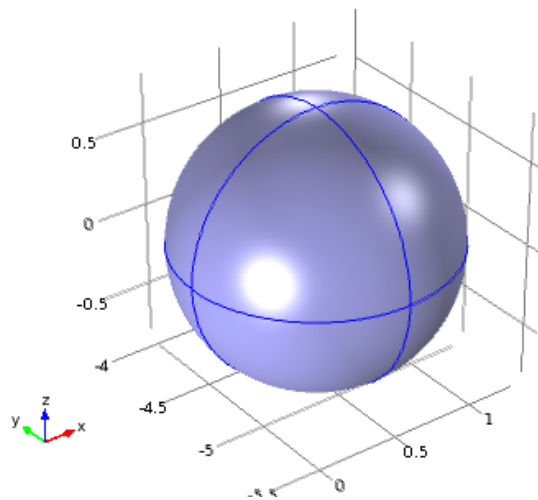
|                        |          |
|------------------------|----------|
| Geometric entity level | Domain   |
| Selection              | Domain 1 |

Settings

Settings

| Description       | Value          |
|-------------------|----------------|
| Type              | Spherical      |
| Center coordinate | {0.5, -4.8, 0} |

**Pressure Acoustics Model 1**



*Pressure Acoustics Model 1*

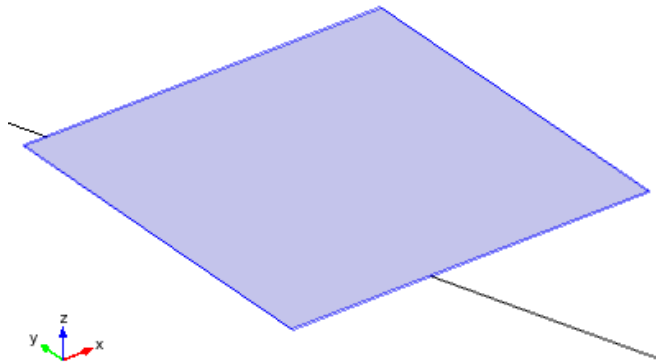
## Selection

|                        |          |
|------------------------|----------|
| Geometric entity level | Domain   |
| Selection              | Domain 1 |

## Settings

## Settings

| Description    | Value        |
|----------------|--------------|
| Density        | User defined |
| Density        | 1.2          |
| Speed of sound | User defined |
| Speed of sound | 343          |

**1.4.6. Boundary Load 1***Boundary Load 1*

## Selection

|                        |             |
|------------------------|-------------|
| Geometric entity level | Boundary    |
| Selection              | Boundary 85 |

## Settings

## Settings

| Description | Value        |
|-------------|--------------|
| Load type   | Total force  |
| Total force | {0, 0, -1.5} |

**1.5. Mesh 1**

## Mesh statistics

| <b>Property</b>         | <b>Value</b> |
|-------------------------|--------------|
| Minimum element quality | 0.05148      |
| Average element quality | 0.7544       |
| Tetrahedral elements    | 111089       |
| Triangular elements     | 13630        |
| Edge elements           | 1815         |
| Vertex elements         | 133          |

**1.5.1. Size (size)**

## Settings

| <b>Name</b>                  | <b>Value</b> |
|------------------------------|--------------|
| Maximum element size         | 0.1          |
| Minimum element size         | 0.0288       |
| Resolution of curvature      | 0.6          |
| Resolution of narrow regions | 0.5          |
| Maximum element growth rate  | 1.5          |
| Custom element size          | Custom       |